Supplementary Information

Tuning the drug multimodal release through a co-assembly strategy based on magnetic gels

Sérgio R. S. Veloso, Ecem Tiryaki, Carlos Spuch, Loic Hilliou, C. O. Amorim, V. S. Amaral, Paulo J. G. Coutinho, Paula M. T. Ferreira, Verónica Salgueiriño*, Miguel A. Correa-Duarte*, and Elisabete M. S. Castanheira*

Experimental

Synthesis procedure of the dehydropeptide

Compound 1 was prepared by synthetic methodologies (see Scheme S1) described elsewhere [18]. ^{1}H and ^{13}C NMR spectra were recorded on a Bruker Avance III at 400 and 100.6 MHz, respectively. DEPT θ 45° and 135°, HMQC and HMBC were used to attribute some signals. Chemical shifts (δ) are reported in parts per million (ppm) and coupling constants (J) are reported in hertz (Hz). Petroleum ether refers to the boiling range of 40-60 °C. Acetonitrile was dried over silica and calcium hydride (CaH_2), and then distilled and stored over molecular sieves. Melting points (°C) were determined in a Gallenkamp apparatus and are uncorrected.

Molecular dynamics

The molecular structure of compound 1 was designed with the program GaussView and optimized geometries of the ground state were obtained from ab initio molecular quantum chemistry calculations, with Gaussian 09 software [1*]. Parametrization was carried out using parameters from the natural amino acids in the GROMOS 54a7 force field [2*,3*]. To validate the proposed parameters, the residues of dehydrophenylalanine and naphthalene acetyl acid were subjected to 12000 steps of energy minimization calculations with the steepest descent algorithm and 100 ps MD simulation in a cubic box solvated with Simple Point Charge (SPC) water model [4*]. Validation was carried out by analyzing the convergence of the system's potential energy and the geometry of the new residues. The compounds were designed and eleven, six or three copies were placed in a cubic box of size 4.5×4.5×4.5 nm solvated with SPC water model [4*]. Each system was energy minimized with the steepest descent algorithm and 60 ns of MD simulations were run, as described in a previous report [30]. The simulation was made in 30×10^6 steps with integration interval of 2 fs. All simulations were run with the GROMACS 5.1.4 software package [5*]. In all MD simulations, the system was maintained at constant temperature and pressure of 310 K and 1 atm, respectively, using the velocity-rescaling thermostat and Berendsen barostat methods [6*], with τ_T = 0.20 ps and τ_P = 0.10 ps. The bond lengths and angles of water

molecules, and the bond lengths and angles of peptides were constrained with the SETTLE and LINCS algorithm [7*,8*]. For the treatment of long-range interactions, the PME method was used with cut-off of 1.4 nm. The van der Waals interactions were also calculated with a cut-off radius of 1.4 nm.

The aggregation properties of each peptide system were evaluated by identifying the occurrence of peptide clusters formed in the simulation box using a cut-off of 0.5 nm between the centre of mass of each peptide [9*]. Visualization of the aggregates was analysed with the PyMOL software.

Synthesis procedure of functionalized magnetic nanoparticles.

Synthesis of magnetic nanoparticles (NPs). Citrate-stabilized iron oxide nanoparticles doped with different metals were synthesized through a co-precipitation method described elsewhere [19,10*]. In general, trisodium citrate dehydrate (1 mmol) and NaOH (4 mmol) were added to 19 mL of ultrapure water at 100 °C. A 1 mL aqueous solution of $FeSO_4.7H_2O$ (1.33 mmol) and the doping metal salt ($MnSO_4.H_2O$, $Ca(CH_3CO_2)_2$ or $MgSO_4$) (0.66 mmol) was added, drop by drop, into the mixture under vigorous agitation and reflux. After 2 h, the solution was cooled down to room temperature, washed through magnetic decantation with water/ethanol 1:1, and dried at 80 °C.

Coating of nanoparticles with APTES (NPs@APTES). The method was adapted from the reference [11*]. Briefly, 150 of mL ethanol, 3 mL of water, 5.1 mL of 5 M ammonium hydroxide and 944 µL of APTES were added in a beaker and kept at 40 °C, while stirring. After 20 min, 6 mL of an aqueous solution of ferrite nanoparticles (4 mg/mL) was added and the reaction was allowed to proceed for 5 h. Nanoparticles were magnetically separated, washed with ethanol and dried at 80 °C.

Functionalization of nanoparticles (NPs@APTES-Phe-NH_2 or NPs@APTES-Phe-L-Phe-NH_2). Fmoc-Phe-OH (1 mmol) was dissolved in DMF (2 mL), and HBTU (1 equiv) and triethylamine (1.2 equiv) were added with 2 min between each addition. The APTES-functionalized nanoparticles dispersed in 2 mL DMF were added and the mixture was left stirring at room temperature (rt) overnight. The particles were washed with ethanol (3×45 mL), and dried to obtained Fmoc-phenylalanine functionalized silica coated nanoparticles. The deprotection was carried out by dispersion in piperidine 20 v/v% in DMF (2 mL) and left stirring for 4 hours. The particles were washed with ethanol (3×45 mL) and left drying at room temperature. The procedure was repeated to obtain Nps@APTES-Phe-L-Phe-NH_2. Quantification of phenylalanine or diphenylalanine per mg of nanoparticle was determined through UV-visible spectroscopy by measuring the amount of Fmoc released [12*]. The first and second coupling of phenylalanine yielded 0.105 ± 0.041 µmol/mg (mass of linked phenylalanine per mass of nanoparticle) and 0.085 ± 0.033 µmol/mg, respectively.

Preparation of liposome formulations and encapsulation efficiency

The used lipids included DPPC (1,2-dipalmitoyl-*sn*-glycero-3-phosphocholine, from Sigma-Aldrich, St. Louis, MO, USA), Ch (cholesterol, from Sigma-Aldrich, St. Louis, MO, USA), DOPE (1,2-dioleoyl-sn-glycero-3-phosphoethanolamine), DOPG (1,2-dioleoyl-*sn*-glycero-3-phospho-(1'-rac-glycerol)), DSPE-PEG (1,2-distearoyl-*sn*-glycero-3-phosphoethanolamine-N-[methoxy(polyethylene glycol)-2000] (ammonium salt)) and egg-PC (egg yolk–phosphatidylcholine, from Sigma-Aldrich, St. Louis, MO, USA). The liposome formulations were prepared by the ethanol injection method using different lipids. Briefly, a 10 mM lipid solution in ethanol was injected, under vigorous agitation, to ultrapure water (400 µL) at 60 °C. The mixture was diluted to a final concentration of 1 mM by addition of water (600 µL) at room temperature. For encapsulation of 5(6)-carboxyfluorescein and doxorubicin, considering the posterior fabrication of lipogels, the lipids ethanolic solution was injected in phosphate buffer 0.1 M pH=7.4 (400 µL) containing 20 mM of 5(6)-carboxyfluorescein or 0.5 mM doxorubicin aqueous (400 µL) solution, respectively, and further diluted for the final volume of 1 mL with water. Regarding the determination of the encapsulation efficiency of doxorubicin and fluorescence assays in gels, the lipids solution was injected in a 0.05 mM doxorubicin aqueous solution (400 µL) and then diluted for a final volume of 1 mL. The encapsulation of DPH was carried out by co-injection (lipid+DPH solution) for a final DPH concentration of 2 µM.

The liposome formulations containing 5(6)-carboxyfluorescein were purified by subjecting the sample to centrifugation at 4000 rpm for 10 min using Amicon® Ultra centrifugal filter units 100 kDa (Merck Millipore, Darmstadt, Germany). Then, the pellet was resuspended in water (1 mL), and the process was repeated for 6 times. The final pellet was resuspended in water (1 mL) and posteriorly used for the preparation of lipogels.

The determination of doxorubicin encapsulation efficiency was carried out by measuring the filtrate's absorbance at wavelength of 580 nm. Three independent measurements were performed for each system and standard deviations (SD) were calculated. The encapsulation efficiency was determined using equation (S1):

$$EE(\%) = \frac{(amount_{total} - amount_{non-encapsulated})}{amount_{total}} \times 100 \quad \text{(S1)}$$

Development of gels

Gelation studies were carried out through turbidity measurements at 500 nm and/or by measuring the fluorescence emission of Nile Red (2 µM, λ_{exc}=520 nm, λ_{em}=620 nm) included in the hydrogel solution

prior to gelation trigger. The hydrogel and glucono-δ-lactone (GdL) concentrations were screened, as well as the effect of preparing through a heating-cooling cycle in phosphate buffer 0.1 M pH=7.4. The GdL-triggered self-assembly was induced by dissolving the compound 1 (structure in Supplementary Information) in basic pH through the addition of 2 v/v% NaOH (1 M) and, then, glucono-δ-lactone was added to decrease the pH homogeneously. The heating-cooling cycle method consisted in dissolving compound 1 in the respective buffer, heating up to 80 °C under agitation until obtaining a translucid solution, and then left cooling at room temperature. Lipogels (liposome-hydrogel formulations) were prepared by the GdL method, which consisted in mixing the liposome formulation solution and compound 1 solution (basic pH) for the required final concentration of both components, and then adding GdL. The same strategy was used for the preparation of magnetic gels and magnetic lipogels. The prepared nanoparticles were added to the hydrogel solution for the final required concentration, from a starting concentrated solution at 10 wt%. All gel solutions were left standing at room temperature until gel phase was attained. Here, the unit wt% stands for m/v%.

Spectroscopic measurements

General methods. Steady-state fluorescence measurements were carried out using a Horiba-Jobin Yvon Fluorolog 3 spectrofluorimeter, equipped with double monochromators in both excitation and emission, Glan-Thompson polarizers and a temperature-controlled cuvette holder. Fluorescence emission spectra were corrected for the instrumental response of the system. The excitation of the hydrogelator was set at 280 nm, and the emission spectrum was collected between 290 nm and 600 nm with a slit of 6 nm in both excitation and emission. Absorption spectra were recorded in a Shimadzu UV-3600 Plus UV-Vis-NIR spectrophotometer. A conventional PAN'alytical X'Pert PRO diffractometer was used for X-ray diffraction (XRD) analyses, operating with Cu K_α radiation, in a Bragg-Brentano configuration. Raman spectroscopy measurements were performed at room temperature with a Renishaw inVia Reflex Raman confocal microscope system (Wotton-under-Edge, United Kingdom), equipped with a high-resolution grating of 1200 grooves mm^{-1}. The excitation line, 785 nm, of a NIR diode laser was focused onto the sample by a x20 objective with a numerical aperture (NA) value of 0.40 in a backscattering geometry. The spectra were acquired with a measured power of about 650 μW on the sample, with a spectral acquisition time of 120 s over one accumulation and the range 100–1800 cm^{-1}. The average hydrodynamic diameter and zeta potential of the nanoparticles (n = 3 independent runs) were measured in a Dynamic Light Scattering (DLS) equipment Litesizer™ 500 (Anton Paar GmbH), using a semiconductor laser diode of 40 mW and λ = 658 nm, backscatter angle (175°), and a controlled temperature of 25 °C.

Fluorescence anisotropy measurements. The steady-state fluorescence anisotropy values, *r*, provide information on the average microviscosity of the gel matrix where the fluorophore is localized and can be determined by equation (S2) [13*],

$$r = \frac{I_{\mathrm{VV}} - GI_{\mathrm{VH}}}{I_{\mathrm{VV}} + 2GI_{\mathrm{VH}}} \quad \text{(S2)}$$

where I_{VV} and I_{VH} are the intensities of the emission spectra obtained with vertical and horizontal polarization, respectively (for vertically polarized excitation light), I_{HV} and I_{HH} are the emission intensities obtained with vertical and horizontal polarization (for horizontally polarized excitation light) and $G = I_{\mathrm{HV}}/I_{\mathrm{HH}}$ is the instrumental correction factor.

Quantification of iron in composites. The method for quantification of iron in nanoparticles was adapted from reference [14*]. Briefly, 1 mg of nanoparticles were digested with HCl 37%. Posteriorly, the solution was diluted to 4.9 M HCl and left stabilize overnight. Standards with different iron concentration in 4.9 M HCl solution were prepared, and the absorbance of all samples was measured at the maximum wavelength (348 nm). Determination of iron content was performed in triplicate.

Characterization techniques

Scanning Transmission Electron Microscopy (STEM). STEM images were recorded using a NanoSEM – FEI Nova 200, operating at 15 kV, coupled to an Electron Dispersive Spectroscopic analyzer (EDS) and Electron Backscatter Diffraction EDAX – Pegasus X4M analyser and detection system (EBSD) at SEMAT/UM (Serviços de Caracterização de Materiais, Guimarães, Portugal). TEM images of nanoparticles were recorded using a high contrast JEOL JEM-1010, operating at 100 kV (CACTI, Vigo, Spain). After preparation of the sample, a small portion was placed onto a TEM 400 mesh copper grid with Formvar/Carbon (ref. S162-4 from Agar Scientific), held by tweezers and the excess solution was cleaned. The processing of STEM images was performed using ImageJ software (National Institutes of Health, NIH, USA), which consisted in enhancing local contrast and adjusting brightness followed by manual selection of fibres.

Magnetic properties. Magnetic measurements were performed in an MPMS3 SQUID magnetometer (Quantum Design). The field-dependent magnetization (hysteresis cycles) of the samples were measured in the large field range (up to 6 kOe or 6T) for each sample, in all the cases at 300 K, given the room temperature applications they are designed for A specific magnetic field correction for the trapped flux in the superconducting coil was conducted, achieving an accuracy of residual less than 2 Oe.

Heat Delivery. With the aim of evaluating the heating performance, magneto-caloric measurements were carried out using a hyperthermia system (magneTherm, nanoTherics) working at f = (262, 270, 381, 616) kHz and at the magnetic field H = (17, 16, 10) mT. For all experiments, the initial temperature was stabilized before starting the measurement. Next, the AC magnetic field was applied for 10 min, and the temperature variation was recorded using a thermocouple.

Rheology. The viscoelastic characterization of gels was performed with a stress-controlled rotational rheometer Anton Paar MCR300. Liquid samples were loaded into the Couette geometry of the rheometer and temperature was kept at 25 °C during testing. The liquid sample was pre-sheared at a shear rate of 5 s^{-1} during one minute to homogenize the sample in the shearing geometry. Then, the gelation kinetics was monitored during 6 h by applying a 0.01% amplitude oscillatory shear at 1 Hz and recording both storage (G') and loss (G") moduli at each second. A sweep in the strain amplitude was performed from 0.001% to 500%, to assess the linear regime of viscoelasticity and the large amplitude oscillatory strain (LAOS) regime.

Drug delivery

Incorporation of doxorubicin. To study the incorporation of doxorubicin in gels through fluorescence spectroscopy, the drug was added to gel's solutions prior to gelation for a final concentration of 10 µM. From the hydrogelator solution, 200 µL were transferred to a fluorescence microcuvette and left standing until the gel was formed. In the case of lipogels, liposomes loaded with 20 µM doxorubicin were prepared and then added 1:1 to a concentrate gel's solutions prior to gelation, thus providing a final concentration of 10 µM doxorubicin.

Drug release. To assess doxorubicin release through fluorescence spectroscopy, gels (200 µL) loaded with 0.1 mM doxorubicin were prepared and left stabilizing overnight in vials. Then, above the gel, pH=7.4 0.1 M phosphate buffer (800 µL) was added to keep pH constant (besides neutralizing the gels), and left standing at room temperature. The AMF was generated in a custom-designed solenoid device (584 turns per meter, length: 28.4 cm and internal diameter: 11.5 cm) by applying an alternating electric current. A magnetic field of 2.09 mT at 100 Hz was used. Aliquots were taken, replaced with fresh buffer and fluorescence was measured to determine the concentration at each time point. Release profile assays were performed in triplicate.

Biological assays

Neuroblastoma cell culture. Human SH-SY5Y neuroblastoma cells were grown at 37 °C, in a humid 5% CO2, in Dulbecco's Modified Eagle's medium (Gibco) supplemented with 10% heat-inactivated fetal

bovine serum (Gibco), 1% antibiotics (penicillin 100 U/mL and streptomycin 100 µg/mL) (Gibco), and 1% l-glutamine (Gibco).

Glioma cell culture. U373 MG human glioma cell cultures were kept at 37 °C and 5% CO_2 under sterile conditions in Dulbecco's modified Eagle's medium (Gibco), supplemented with 10% fetal bovine serum (Gibco, plus 1% antibiotics (penicillin 100 U/mL and streptomycin 100 µg/mL) (Gibco).

Cell culture treatment. The cell cultures were treated for 24 hours and 48 hours with nanoparticles 10, 20, 50 and 100 µg/mL. Positive control was H_2O_2 100 µM.

Cell viability. The effect of different designs of nanoparticles on the survival of U373 human glioma cells and SH-SY5Y human neuroblastoma were determined by the MTT assay (3-[4,5-dimethylthiazol-2-yl]-2,5-diphenyltetrazolium bromide), using the Cell Proliferation Kit I (Roche Diagnostics, Mannheim, Germany). The cells were seeded in a 96-well plate at a density of 105 cells/well in DMEM. Twenty-four hours later, the cells were treated with nanoparticles at the concentrations described above; untreated cells were used as controls. After incubation for 24 h and 48 h, a cell viability assay was performed as described in the MTT assay protocol.

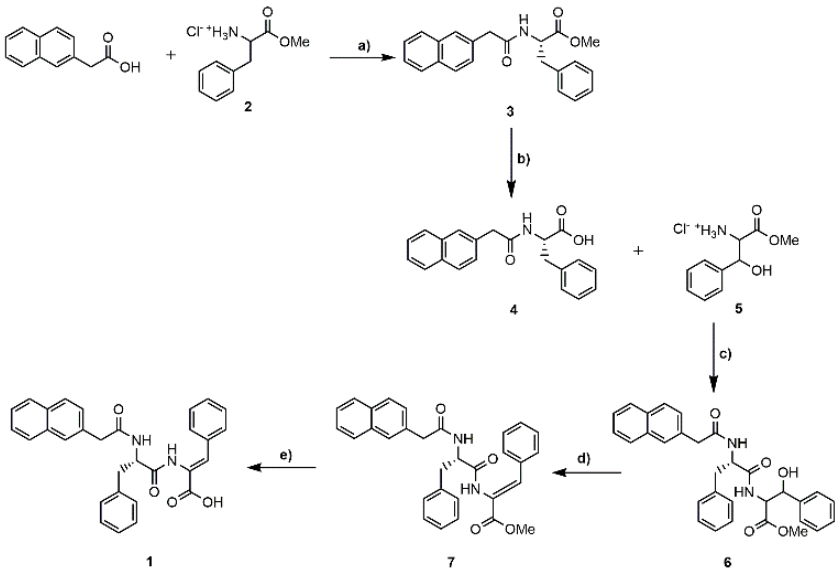

Scheme S1. Synthesis of compound **1**. a) DCC, HOBt, Et_3N, ACN, rt; b) (1) NaOH (1 M), methanol, rt, (2) $KHSO_4$; c) DCC, HOBt, Et_3N, ACN, rt; d) (1) Boc_2O, DMAP, dry ACN, rt (2) TMG; e) (1) NaOH (1 M), 1,4-dioxane, rt, (2) $KHSO_4$.

Synthesis of the methyl ester of phenylalanine [H-D,L-Phe-OMe (2)]: Phenylalanine [H-D,L-Phe-OH] (31.8 mmol, 5.26 g) was added to methanol for a final concentration of 1 M in an ice bath. Thionyl chloride (3.4 equiv) was added dropwise and the reaction mixture was left stirring for 8 h at 40 °C. The solvent was removed under reduced pressure and ethyl ether was added. The process was repeated until a white solid of compound **2** was formed. (98%, 6.72 g).

^{1}H NMR (400 MHz, DMSO-d_6) δ: 3.09 (1H, dd, J = 7.4 and 14.0 Hz, *β*-CH), 3.20 (1H, dd, J = 5.6 and 14.0 Hz, *β*-CH), 3.64 (3H, s, OCH_3), 4.22 (1H, t, J = 6 and 7.4 Hz, *α*-CH), 7.22-7.34 (5H, m, Ar H), 8.74 (3H, s, NH^{3+}).

Synthesis of the methyl ester of *N*-2-naphtylacetyl-L-phenylalanine [2-Naph-L-Phe-OMe (3)]: 2-Naphthylacetic acid (0.93 g, 5 mmol) was dissolved in acetonitrile (10 mL $mmol^{-1}$) and put in an ice bath. HOBt (1.10 equiv), DCC (1.10 equiv), H-D,L-Phe-OMe (1.10 equiv), and triethylamine (2.10 equiv) were added with 2 min between each addition. The mixture was left stirring at rt overnight. The urea was filtered, and the solvent removed under reduced pressure. Acetone was added, and the mixture was stored in the freezer for 2 h. The urea was filter again. Evaporation at reduced pressure gave a residue that was partitioned between ethyl acetate (30 mL) and $KHSO_4$ (30 mL, 1M). The organic phase was thoroughly washed with $KHSO_4$ (1M, 2 x 30 mL), $NaHCO_3$ (1M, 2 x 30 mL) and brine (3 x 30 mL) and dried with $MgSO_4$. Removal of the solvent afforded compound **3** (95%, 1.65 g).

^{1}H NMR (400 MHz, $CDCl_3$) δ: 3.01 (2H, dq, J = 5.6 and 14.0 Hz, *β*-CH_2), 3.70 (3H, s, OCH_3), 3.72 (2H, s, CH_2), 4.84-4.88 (1H, m, *α*-CH), 5.83 (1H, d, J = 7.2 Hz, NH), 6.78-6.81 (2H, m, ArH Phe), 6.99 (2H, t, J = 8.0 Hz, ArH Phe), 7.10 (1H, tt, J = 2.0 and 7.4 Hz, ArH Phe), 7.3 (1H, dd, J = 1.6 and 8.4 Hz, ArH Naph), 7.49-7.54 (2H, m, ArH Naph), 7.66 (1H, s, H Naph), 7.79-7.87 (3H, m, ArH Naph).

Synthesis of *N*-2-naphtylacetyl-L-phenylalanine [2-Naph-L-Phe-OH (4)]: The 2-Naph-L-Phe-OMe (1.65 g, 4.75 mmol) was dissolved in methanol (10 mL $mmol^{-1}$) and a solution of NaOH 1 M (1.5 equiv) was added. The reaction was followed by TLC until no starting material was detected. The organic solvent was removed under reduced pressure, and the reaction mixture was acidified to pH 2-3 with $KHSO_4$ (1 M). The solid was filtered and washed with ethyl ether. The solid was identified as 2-Naph-L-Phe-OH, **4** (1.4 g, 91 %).

^{1}H NMR (400 MHz, DMSO-d_6) δ: 2.84-2.90 (1H, m, *β*-CH_2), 3.04-3.08 (1H, m, *β*-CH_2), 3.53-3.62 (2H, m, CH_2), 4.39-4.44 (1H, m, *α*-CH), 7.18 (5H, s, ArH), 7.25-7.28 (1H, dd, J = 1.6 and 8.4 Hz, ArH), 7.43-7.49 (2H, m, ArH), 7.64 (1H, s, ArH), 7.76-7.80 (2H, m, ArH), 7.84-7.86 (1H, d, J = 8.0 Hz, ArH), 8.38 (1H, d, J= 8.0 Hz, NH), 12.60 (1H, s, CO_2H);

Synthesis of the methyl ester of *β*-hydroxyphenylalanine [H-D,L-Phe(*β*-OH)-OMe (5)]: The *β*-hydroxyphenylalanine [H-D,L-Phe(*β*-OH)-OH] (30 mmol, 5.44 g) was added for a final concentration of 1 M in an ice bath. Thionyl chloride (3.4 equiv) was added dropwise and the reaction mixture was left stirring for 8 h at 40 °C. The solvent was removed under reduced pressure and ethyl ether was added. The process was repeated until a white solid of compound **5** was formed (98%, 5.74 g).

^{1}H NMR (400 MHz, DMSO-d_6) δ: 3.60 (3H, s, OCH_3); 4.15 [1H, d, α-CH Phe(*β*-OH)]; 5.01-5.02 [1H, t, *β*-CH Phe(*β*-OH)]; 6.56 [1H, brs, J = 4.4 Hz, OH Phe(*β*-OH)]; 7.31-7.38 [5H, m, ArH Phe(*β*-OH)]; 8.45 [3H, s, NH_3^+ Phe(*β*-OH)].

Synthesis of the methyl ester of *N*-2-naphtylacetyl-L-phenylalanine-*β*-hydroxyphenylalanine [2-Naph-L-Phe-D,L-Phe(*β*-OH)-OMe (6)]: 2-Naph-L-Phe-OH (1.4 g, 4.2 mmol) was dissolved in acetonitrile (10 mL $mmol^{-1}$) and put in an ice bath. HOBt (1.10 equiv), DCC (1.10 equiv), H-D,L-Phe-OMe (1.10 equiv), and triethylamine (2.10 equiv) were added with 2 min between each addition. The mixture was left stirring at rt overnight. The urea was filtered, and the solvent removed under reduced pressure. Acetone was added, and the mixture was stored in the freezer for 2 h. The urea was filter again. Evaporation at reduced pressure gave a residue that was partitioned between ethyl acetate (30 mL) and $KHSO_4$ (30 mL, 1M). The organic phase was thoroughly washed with $KHSO_4$ (1M, 2 x 30 mL), $NaHCO_3$ (1M, 2 x 30 mL)

and brine (3 x 30 mL) and dried with $MgSO_4$. Removal of the solvent afforded compound **6** as a diastereomeric mixture (76.1%, 1.63 g).

^{1}H NMR (400 MHz, $CDCl_3$) δ: 2.6-2.7 (1H, m, *β*-CH Phe), 2.80-2.85 (2H, m, 2×*β*-CH Phe), 2.9 (1H, m, *β*-CH Phe), 3.61 (4H, s, 2×CH_2 Naph), 3.69 [6H, s, 2×OCH_3 Phe(*β*-OH)], 4.66-4.83 [4H, m, 4×*α*-CH Phe and Phe(*β*-OH)], 5.22 [1H, d, J = 3.2 Hz, *β*-CH Phe(*β*-OH)], 5.28 [1H, d, J = 3.2 Hz, *β*-CH Phe(*β*-OH)], 5.88 (1H, m, NH), 5.99 (1H, m, NH), 6.60-6.64 (2H, m, ArH), 6.80-7.34 (22H, m, 16×ArH, 2×NH), 7.40-7.6 (6H, m, ArH), 7.7-7.9 (6H, m, ArH).

Synthesis of the methyl ester of *N*-2-naphtylacetyl-L-phenylalanine-*Z*-dehydrophenylalanine [2-Naph-L-Phe-Z-ΔPhe-OMe (7)]: To a solution of compound **6** in dry acetonitrile (10 mL, 1 M) DMAP (0.1 equiv) and Boc_2O (1 equiv) were added under rapid stirring at rt. The mixture was monitored by ^{1}H NMR until all reactant was consumed. *N,N,N',N'*-tetramethylguadinine (2 % in volume, 0.2 mL) was added under continued stirring. The mixture was left stirring at rt and monitored by ^{1}H NMR until all reactant was consumed. The precipitate was filtered and identified as compound **7** (0.99 g, 63%).

^{1}H NMR (400 MHz, $CDCl_3$) δ: 2.94-3.01 (2H, m, *β*-CH_2 Phe), 3.68 (2H, s, CH_2 Naph), 3.80 (3H, s, OCH_3), 4.78-4.84 (1H, m, α-CH), 5.92 (1H, d, J = 7.6 Hz, NH Phe), 6.97-7.18 (6H, m, 6×ArH), 7.27-7.38 (7H, m, 7×ArH), 7.50-7.56 (2H, m, ArH and *β*-CH ΔPhe), 7.75-7.86 (4H, m, 3×ArH and NH ΔPhe).

Synthesis of the *N*-2-naphtylacetyl-L-phenylalanine-*Z*-dehydrophenylalanine [2-Naph-L-Phe-*Z*-ΔPhe-OH (1)]: Compound **7** (0.99 g, 2.3 mmol) was dissolved in 1,4-dioxane (10 mL mmol^{-1}) and a solution of NaOH 1 M (3 equiv) was added. The reaction was followed by TLC until no starting material was detected. The organic solvent was removed under reduced pressure, and the reaction mixture was acidified to pH 2-3 with $KHSO_4$ (1 M). The solid was filtered and washed with ethyl ether. The solid was identified as 2-Naph-L-Phe-Z-ΔPhe-OH, **1** (1.02 g, 90 %).

^{1}H NMR (400 MHz, DMSO-d_6) δ: 2.77-2.83 (1H, m, *β*-CH), 3.12-3.17 (1H, m, *β*-CH), 3.54-3.62 (2H, m, CH_2 Naph), 4.58-4.63 (1H, m, *α*-CH Phe), 6.96 (1H, s, *β*-CH ΔPhe), 7.05-7.46 (13H, m, Ar H), 7.62 (1H, s, Ar H), 7.71-7.85 (3H, m, Ar H), 8.59 (1H, d, J = 8.8 Hz, NH Phe), 9.73 (1H, s, NH ΔPhe);

^{13}C NMR (100.6 MHz, DMSO-d_6) δ: 37.16 (*β*-CH_2 Phe), 42.18 (CH_2 Naph), 54.14 (*α*-CH Phe), 125.43 (CH), 125.95 (CH), 126.27 (CH), 126.54 (*α*-C ΔPhe), 127.19 (CH), 127.33 (CH), 127.41 (CH), 127.57 (CH), 128.02 (CH), 128.46 (CH), 129.18 (CH), 129.25 (CH), 129.93 (CH), 131.70 (C), 131.93 (*β*-CH ΔPhe), 132.89 (C), 133.54 (C), 133.94 (C), 137.85 (C Phe), 166.19 (C=O ΔPhe), 170.06 (C=O Phe), 171.16 (C=O Naph); HRMS (ESI) *m/z*: $[M+H]^+$ calcd for $C_{30}H_{27}N_2O_4^+$ 479.19653; found, 479.19627. Mp: 165.0-167.0 °C.

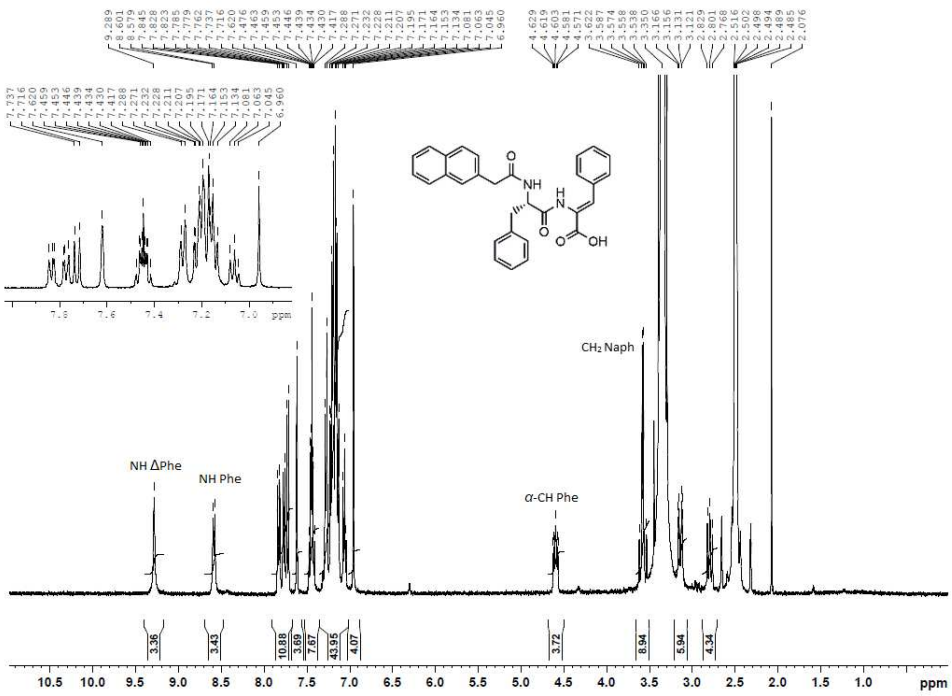

Figure S1. ^{1}H NMR spectrum of 2-Naph-L-Phe-*Z*-ΔPhe-OH, **1** in DMSO-d_6.

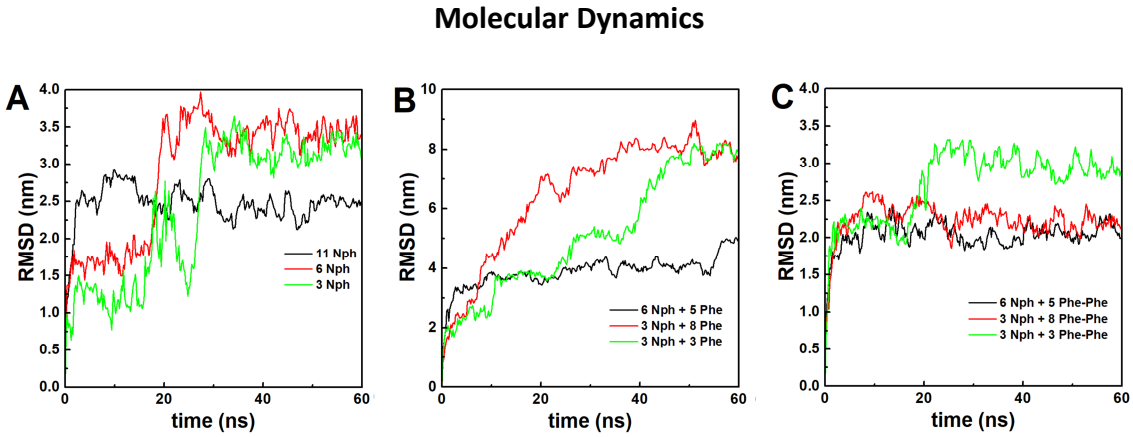

Figure S2. Root-mean-square deviation (RMSD) of the 2-Naph-L-Phe-*Z*-ΔPhe-OH (Nph) dehydropeptides without (A) and with (B) phenylalanine (Phe) and (C) diphenylalanine (Phe-Phe).

Figure S3. Molecular dynamics assays snapshots over the 60 ns. Legend: Nph: 2-Naph-L-Phe-*Z*-ΔPhe-OH (green); Phe: phenylalanine (blue); Phe-Phe: diphenylalanine (yellow).

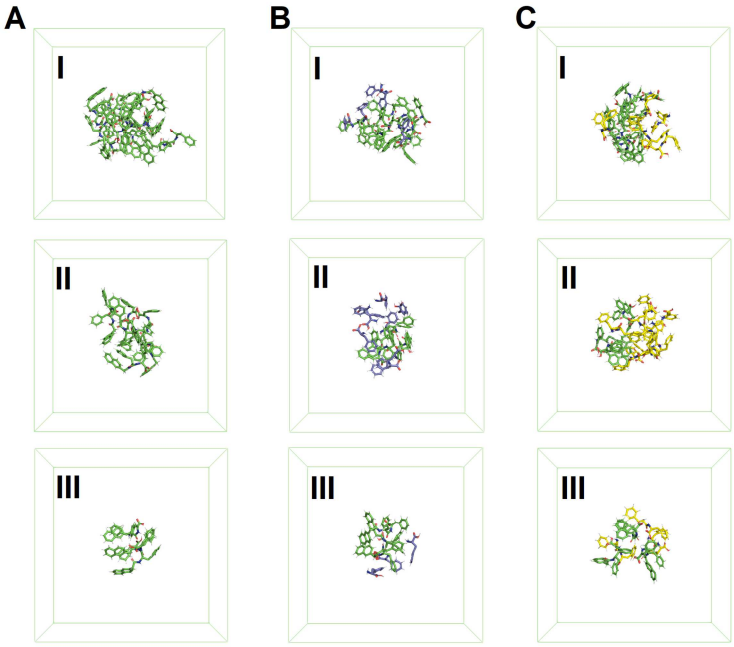

Figure S4. Representative molecular dynamics structures of the aggregates containing: (AI) 11, (AII) 6 and (AIII) 3 dehydropeptide (Nph, green) molecules; (BI) 6 Nph and 5 phenylalanine (Phe(R), blue), (BII) 3 Nph and 8 Phe, and (BIII) 3 Nph and 3 Phe; (CI) 6 Nph and 5 diphenylalanine (Phe-Phe(R), yellow), (CII) 3 Nph and 8 Phe-Phe, and (CIII) 3 Nph and 3 Phe-Phe.

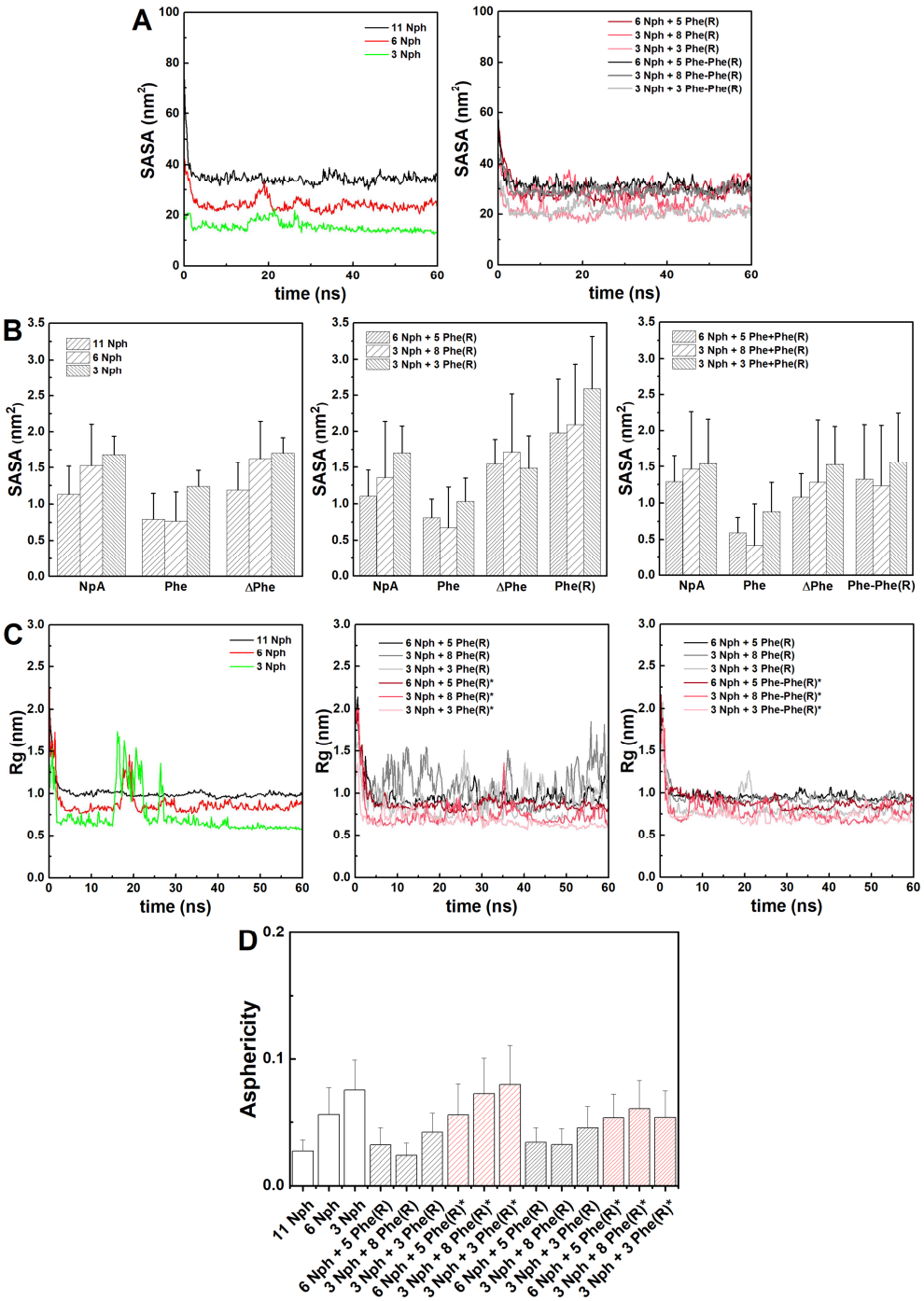

Figure S5. (A) Average solvated surface area over time of the systems. Legend: Nph: 2-Naph-L-Phe-*Z*-ΔPhe-OH; Phe: phenylalanine; ΔPhe: Dehydrophenylalanine; Phe-Phe: diphenylalanine; "(R)": residue added. (B) Average solvated surface area of the dehydropeptide residues. (C) Radius of gyration of the aggregate over time. Legend: *: without phenylalanine contribution. (D) Asphericity of the aggregates averaged over the 60 ns of dynamic simulation. The asphericity is defined as $r_{gz}^2 - 0.5(r_{gx}^2 + r_{gy}^2)$, where r_{gz}^2, r_{gx}^2 and r_{gy}^2 are the ordered principal moments of the gyration tensor so that $r_{gz}^2 > r_{gy}^2 > r_{gx}^2$, which is zero for a spherical shape and aspherical for values higher than zero [31,32].

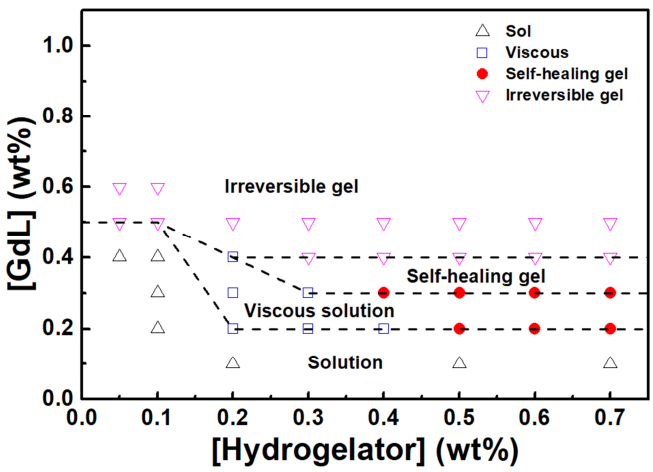

Figure S6. Phase transition diagram of the hydrogelator prepared through addition of GdL to a basic hydrogelator solution (2 V/V% NaOH 1M).

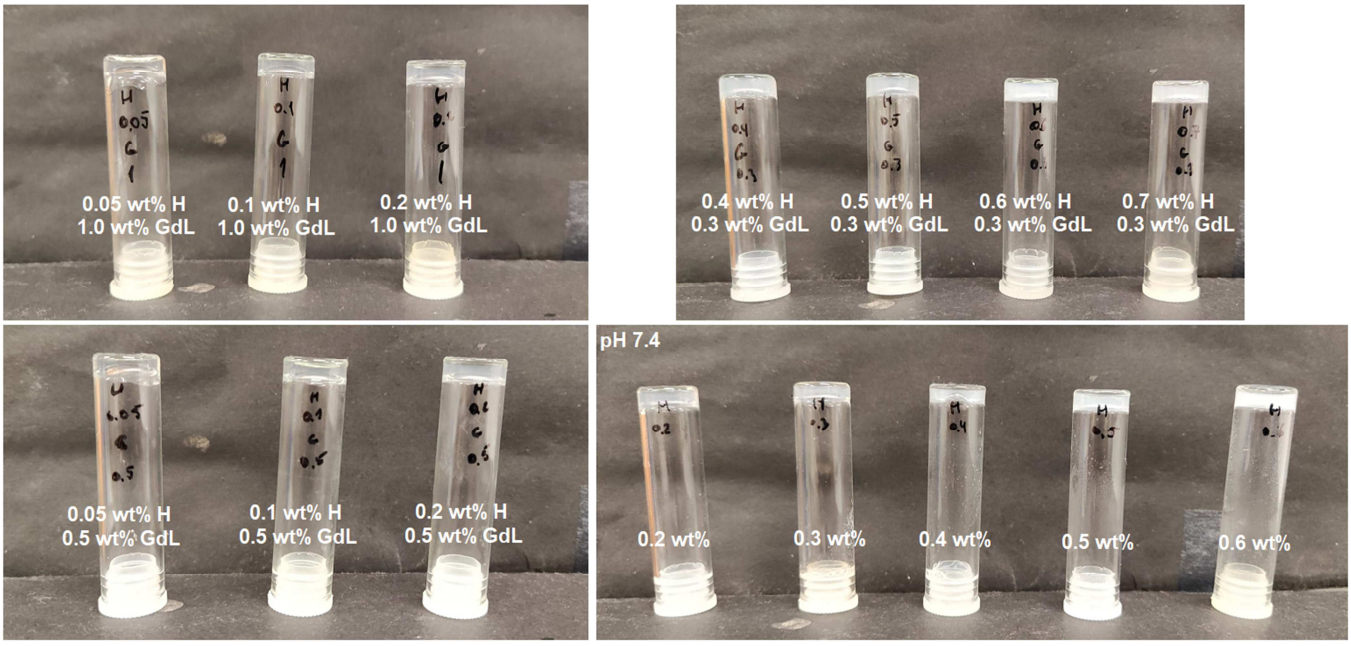

Figure S7. Images of hydrogels prepared through addition of GdL and through a heating-cooling cycle in pH=7.4 phosphate buffer.

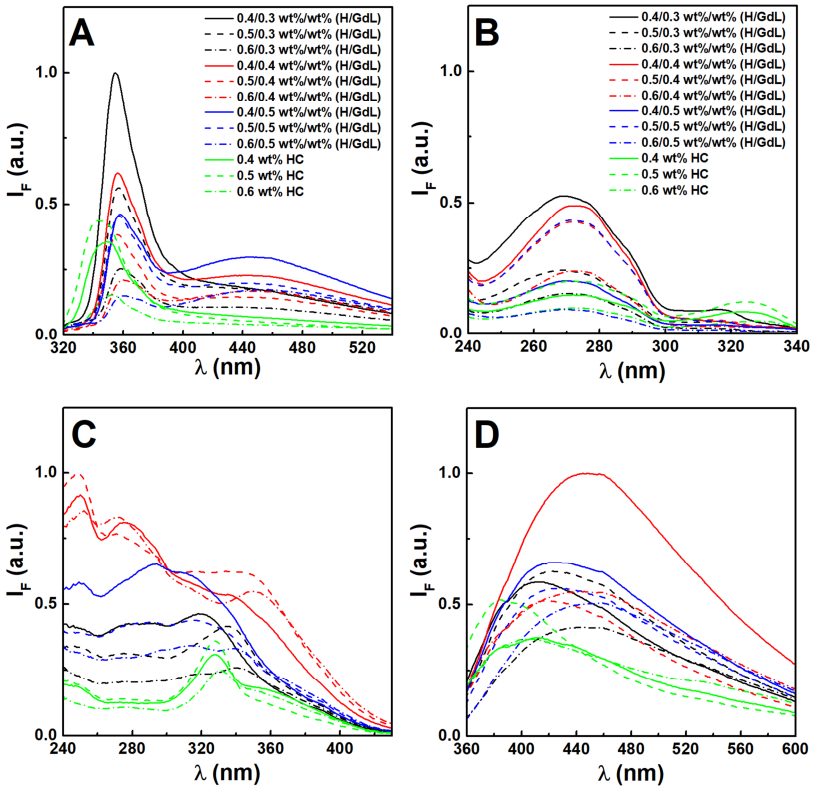

Figure S8. (A) Fluorescence emission spectra of hydrogels aromatic moieties directly excited (λ_{exc}=280 nm) at different hydrogelator-to-GdL ratios (H/GdL), and prepared through heating-cooling cycle (HC). Fluorescence excitation spectra of the (B) monomer band at 360 nm and (C) aggregates band at 450 nm at different hydrogelator-to-GdL ratios (H/GdL), and prepared through heating-cooling cycle (HC). (D) Fluorescence emission of the hydrogels aggregates through excitation at 340 nm. The difference in the excitation spectra of the bands centred at 360 nm and 450 nm demonstrate that different species contribute for each emission.

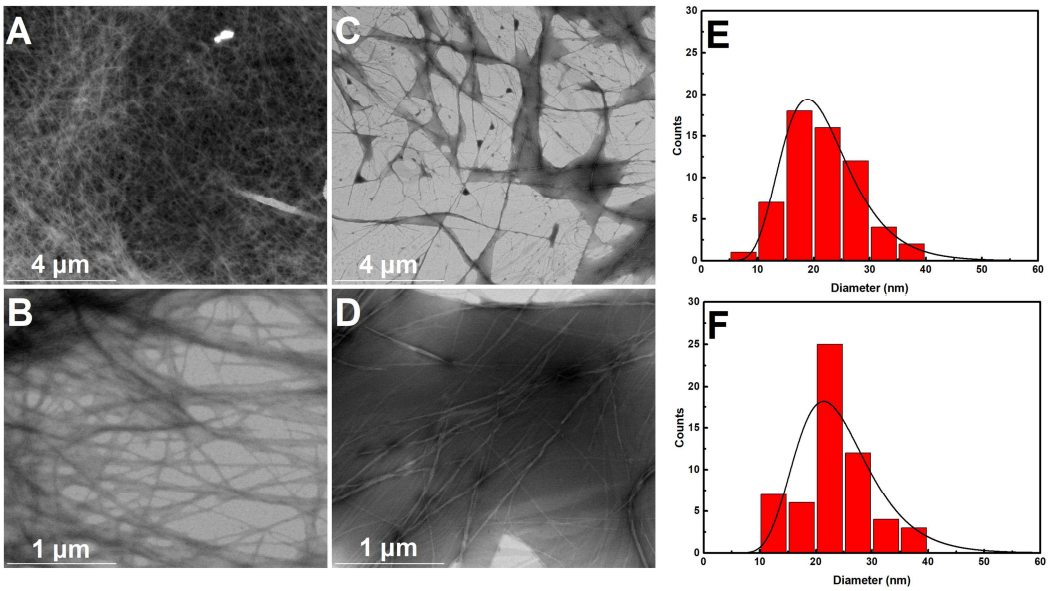

Figure S9. STEM images of hydrogels prepared at 0.5 wt% of hydrogelator through (A,B) the GdL (0.4 wt%) method and (C,D) heating-cooling cycle method (phosphate buffer pH=7.4). Size histograms of the hydrogels prepared through (E) GdL method and (F) heating-cooling cycle method fitted to a lognormal function.

The aggregates fraction, $f(t)$, is defined as follows:

$$f(t) = \frac{S_{obs} - S_{free}}{S_{agg} - S_{free}} \quad \text{(S3)}$$

where S_t, S_{free} and S_∞ stand for the measured signal (turbidity measured at 500 nm or Nile Red fluorescence emission) observed at time t, before addition of GdL and when aggregated (signal at $t = 8\ h$), respectively.

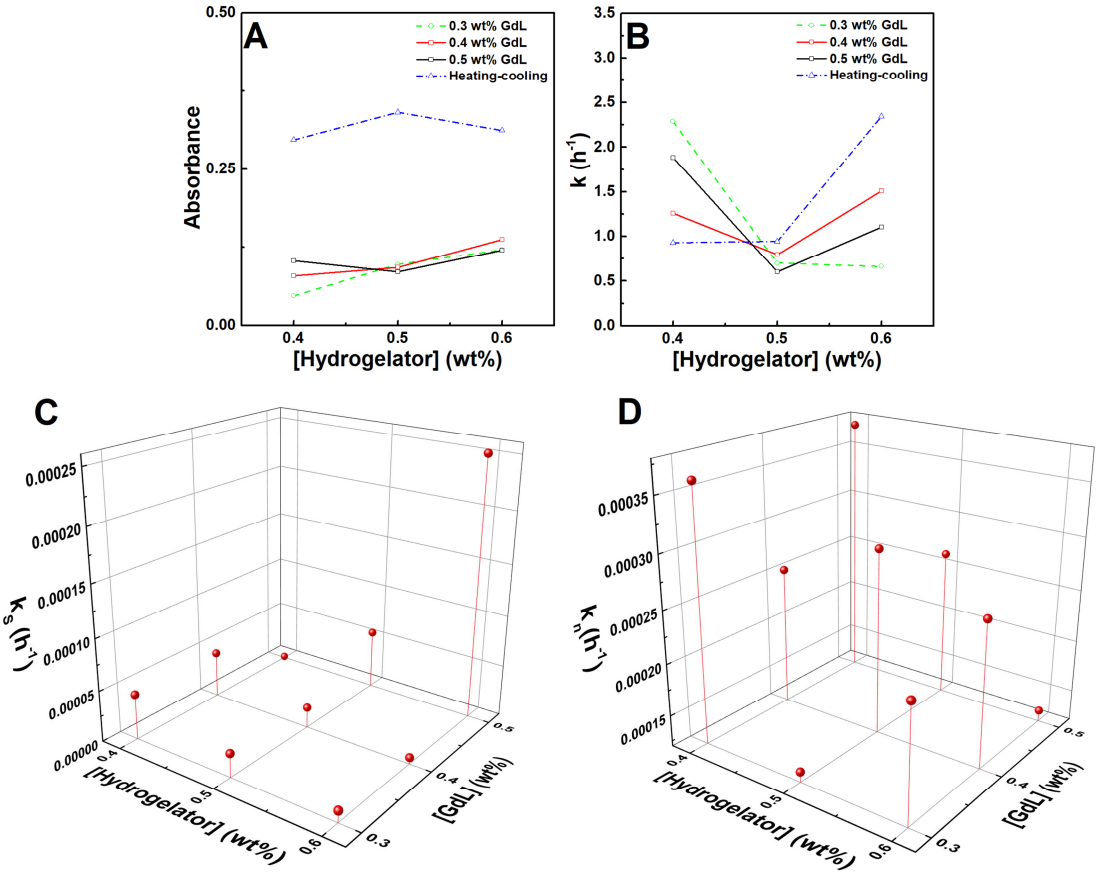

Figure S10. (A) Absorbance at 500 nm of hydrogels prepared through the GdL addition and heating-cooling cycle methods. (B) Dependence of the turbidity kinetics rate constant, k_{emp}, on the hydrogelator concentration obtained from the fitted sigmoidal model $T(t) = \frac{T(\infty)}{\sqrt[v]{(1+ve^{-k_{emp}(t-t_m)})}}$, where $T(t)$ is the turbidity at time t, $T(\infty)$ is the final turbidity, and t_m is the point of the maximum elongation rate (v is considered 1). (C,D) Kinetic parameters obtained from the fitting of the Saitô's fractional aggregation model to the fluorescence kinetics data. The parameter k_s is the effective growth rate, and k_n is the nucleation rate.

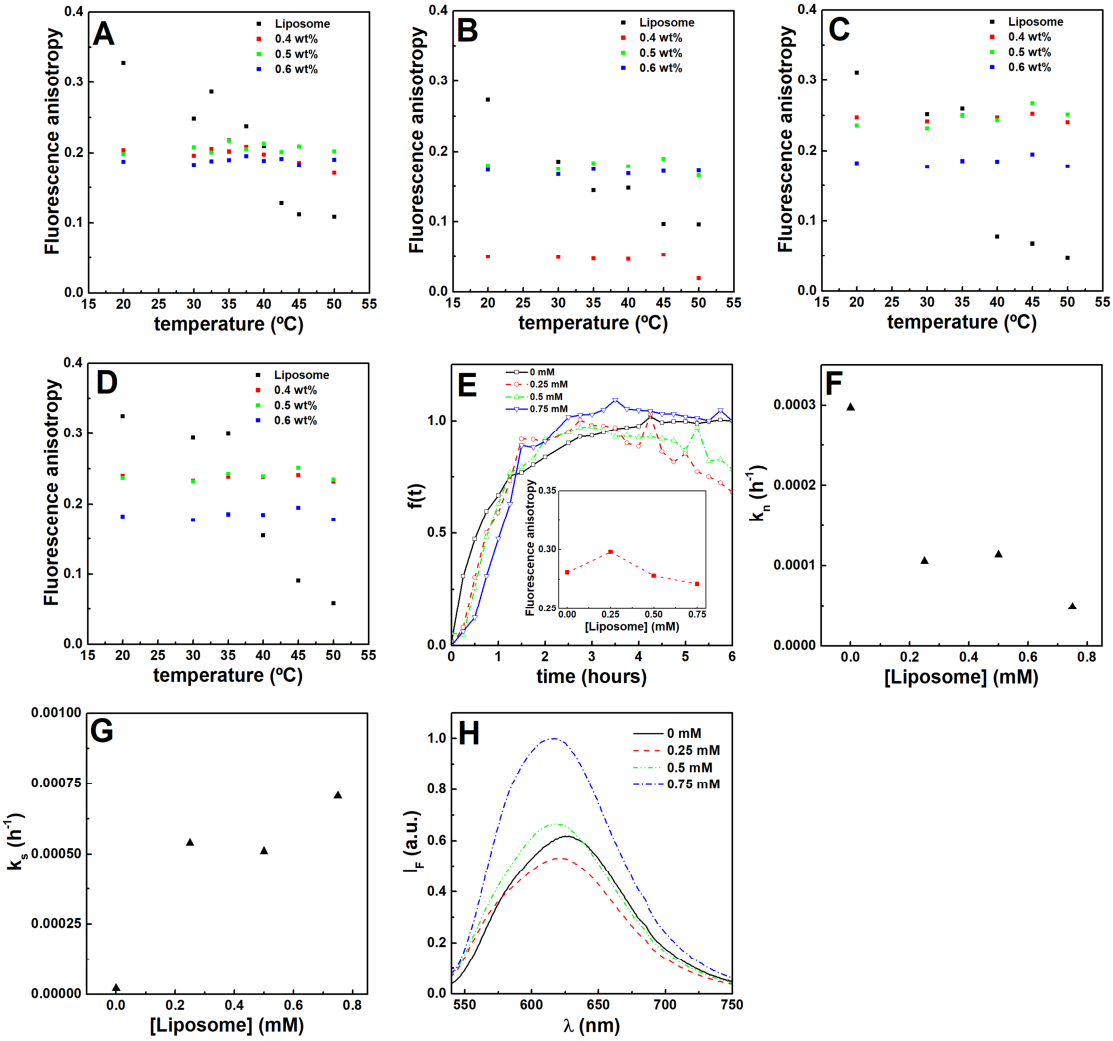

Figure S11. Temperature dependence of fluorescence anisotropy (*r*) of DPH (2 µM) loaded in liposomes of (A) DPPC, (B) PC:Ch (7:3), (C) DPPC:DOPG (9:1) and (D) DPPC:DOPE (9:1) incorporated in hydrogels at various concentration. (E) Fluorescence emission kinetics of hydrogel loaded with Nile Red (2 µM, λ_{exc}=520 nm, λ_{em}=620 nm) and various concentrations of liposomes. Inset: Nile Red fluorescence emission anisotropy dependence on DPPC:PEG (19:1) liposome content. (F,G) Nucleation (k_n) and effective growth (k_s) rate of fluorescence kinetics dependence on DPPC:PEG (19:1) liposome content in gels prepared at 0.5 wt% hydrogelator and 0.4 wt% GdL, and (H) the respective fluorescence emission of Nile Red (2 µM, λ_{exc}=520 nm, λ_{em}=620 nm).

Table S1. Hydrodynamic size (HD), polydispersity index (PDI), zeta potential of DPPC:Ch:PEG 17:2:1 and DPPC:PEG 19:1 liposome formulations at 25 °C and 45 °C. The doxorubicin fluorescence anisotropy (r) of the lipogel formulations was also included. SD: standard deviation.

	25 °C				45 °C	
	HD ± SD (nm)	**PDI ± SD**	**Zeta potential ± SD (mV)**	**r**	**HD ± SD (nm)**	**PDI ± SD**
DPPC:Ch:PEG 17:2:1	108.5 ± 7.9	0.238 ± 0.003	-22.89 ± 0.41	0.15	116.6 ± 1.3	0.245 ± 0.009
DPPC:PEG 19:1	193.8 ± 24.4	0.228 ± 0.008	-36.91 ± 0.68	0.17	145.8 ± 5.8	0.237 ± 0.006
DPPC:Ch:PEG 17:2:1 Lipogel	--	--	--	0.23	--	--
DPPC:PEG 19:1 Lipogel	--	--	--	0.22	--	--
Hydrogel	--	--	--	0.26	--	--

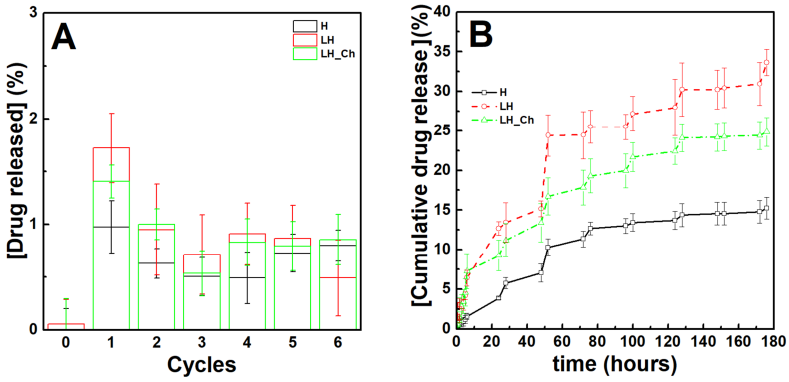

Figure S12. (A) Heat-triggered doxorubicin release per cycle from the hydrogel and lipogels containing DPPC:Ch:PEG 17:2:1 or DPPC:PEG 19:1. (B) Cumulative doxorubicin release from the hydrogel and lipogels containing DPPC:Ch:PEG 17:2:1 or DPPC:PEG 19:1 subjected to higher contribution from erosion at 25 °C. Each cycle of heating (45 °C) was carried out for 1 h with an interval of 24 h and the first cycle was initiated after 48 h of passive release. Legend: LH_Ch: Lipogel with DPPC:Ch:PEG 17:2:1 liposomes; LH: Lipogel with DPPC:PEG 19:1 liposomes; H: hydrogel.

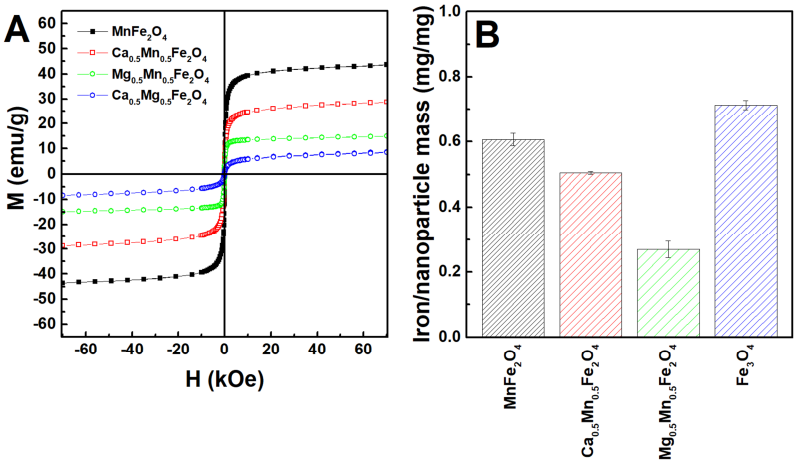

Figure S13. (A) Field-dependent magnetization of the synthesized nanoparticles with saturation magnetization (M_S) values correlated with the nominal synthesis stoichiometric values. (B) Iron mass per mass of nanoparticle of the samples with the highest values of M_S and comparison with iron content of magnetite (Fe_3O_4) obtained by the same method.

Table S2. Coercive field (H_c), saturation magnetization (M_s), remnant magnetization (M_r), and ratio M_r/M_s for calcium, magnesium and manganese doped ferrite nanoparticles (nominal synthesis stoichiometry), at room temperature (T=300 K), ratio of mass of iron with respect to the mass of nanoparticles (mg/mg) and the experimental iron stoichiometry estimate.

	H_c (Oe)	M_s (emu/g)	M_r (emu/g)	M_r/M_s	Iron/nanoparticle (mg/mg)	Iron stoichiometry
$MnFe_2O_4$	33	43.6	3.6	0.08	0.61 ± 0.02	2.55 ± 0.08
$Ca_{0.5}Mn_{0.5}Fe_2O_4$	12.0	28.7	0.4	0.01	0.51 ± 0.01	2.12 ± 0.02
$Mg_{0.5}Mn_{0.5}Fe_2O_4$	3.7	15.0	0.1	0.01	0.27 ± 0.03	1.13 ± 0.11
$Ca_{0.5}Mg_{0.5}Fe_2O_4$	34.3	8.7	0.2	0.02	-	-
Fe_3O_4	-	-	-	-	0.71 ± 0.01	3

X-Ray Diffraction Parameters

A Rietveld analysis was performed using a phase adapted from a CIF file of iron oxide (CIF file 2300618) space group Fd-3m) by substituting iron by manganese (and calcium) with an inversion of 0.6 as reported for other manganese ferrites [12]. The diffraction peaks of the $MnFe_2O_4$ crystalline structure are observed at 2θ = 18.2 (1 1 1), 29.9° (2 2 0), 35.3° (3 1 1), 36.9° (2 2 2), 42.9° (4 0 0), 53.2° (4 2 2), 56.6° (3 3 3) and (5 1 1), 62.2° (4 4 0), 65.4° (5 3 1), 70.6° (6 2 0), 73.6° (5 3 3), 74.6° (6 2 2), 78.5° (4 4 4), 86.2° (6 4 2), 89.1° (7 3 1) and (5 5 3), and the diffraction peaks of the calcium-doped are at 2θ = 18.3 (1 1 1), 30.0° (2 2 0), 35.4° (3 1 1), 37.0° (2 2 2), 43.0° (4 0 0), 53.3° (4 2 2), 56.9° (3 3 3) and (5 1 1), 62.4° (4 4 0), 65.6° (5 3 1), 70.8° (6 2 0), 73.8° (5 3 3), 74.8° (6 2 2), 78.8° (4 4 4), 86.6° (6 4 2), 89.6° (7 3 1) and (5 5 3).

Table S3. X-ray diffraction Rietveld refinement calculated parameters Bragg R-factor (R_B) R_F-factor (R_F), χ^2 and phase sizes.

Nanoparticles	Phase size (nm)	Lattice Constant (Å)	R_F	R_B	χ^2
Manganese ferrite	9.20	8.433	4.54	4.72	0.90
Calcium-doped manganese ferrite	4.70	8.408	6.16	5.66	1.23

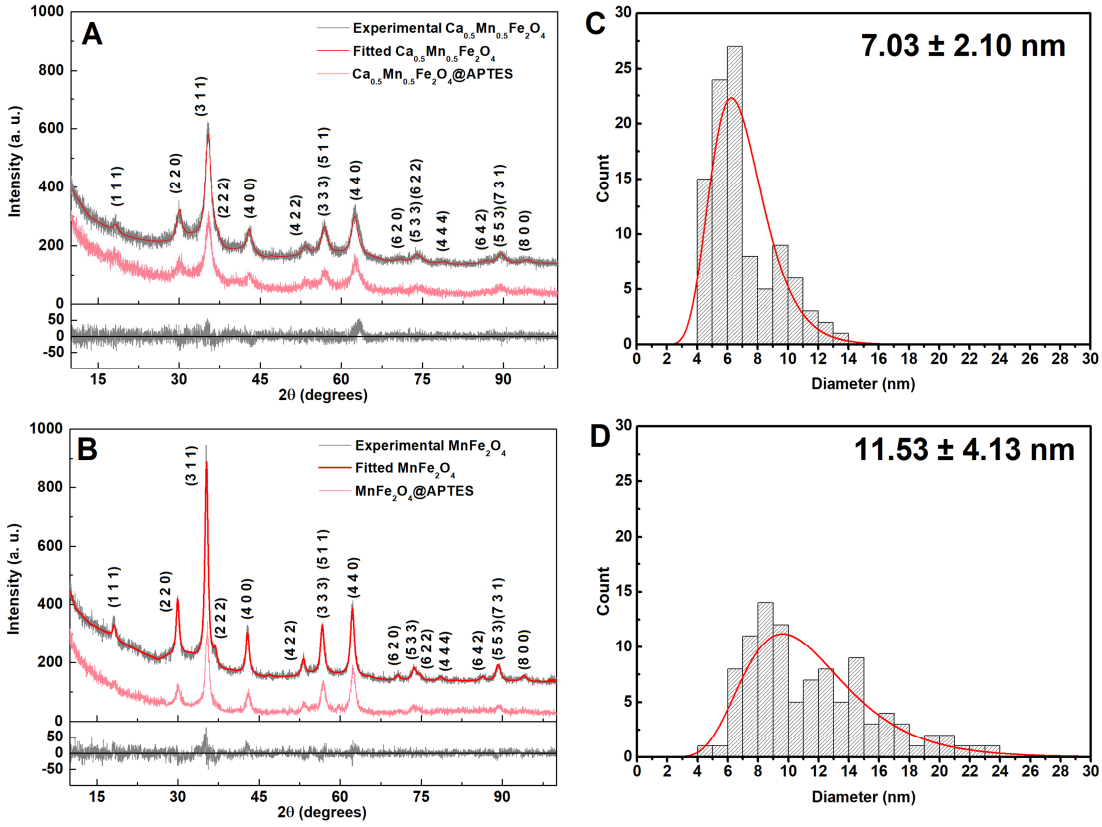

Figure S14. (A,B) X-ray diffraction patterns of the calcium-doped and manganese ferrites with and without APTES. The bottom grey line corresponds to the mismatch from the fitting of the experimental profile of nanoparticles without APTES. (C,D) Size histogram of the respective APTES-coated magnetic nanoparticles fitted to a lognormal distribution. The particles are identified according to the nominal stoichiometry used in synthesis.

Raman analysis (100-800 cm^{-1} range) of (calcium-doped) manganese ferrite

The Raman spectra of ferrites is characterized by five major bands as predicted by the group theory for spinels with *Fd3m* space group: the A_{1g} band, E_g band, and three T_{2g} bands. Lorentzian curves were fitted to deconvolute the multiple contributions for each band (figure S15). The Fe_3O_4 A_{1g} band is centred around 670 cm^{-1}. The shoulder displayed at ~715 cm^{-1} (band in orange) that can be associated with the presence of maghemite (γ-Fe_2O_3), cation vacancies or other order/disorder features [37,38].

The manganese ferrite additional A_{1g} band contributions stems from the distribution of Fe and Mn cations in the tetrahedral positions. Besides the band ~600 cm^{-1}, the contribution at ~640 cm^{-1} suggests the oxidation of some manganese cations to Mn^{3+} [37]. Doping with calcium led to additional contributions, confirming the occupation of some (likely tetrahedral) sites by calcium cations.

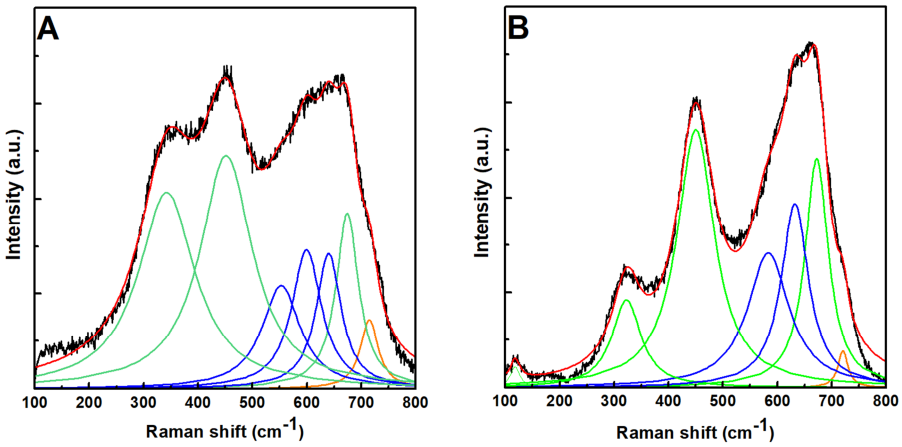

Figure S15. Raman scattering spectra of the (A) calcium-doped manganese ferrite and (B) manganese ferrite nanoparticles.

Functionalized nanoparticles magnetic properties

The Raman spectra **(1100-1800 cm^{-1} range)** of the functionalized nanoparticles display peaks which can be assigned to characteristic frequencies of phenylalanine, mainly associated with the side-chain C-C, N-C and CH_2 vibration modes, besides NH_3^+ symmetric bending and rocking (~1450 cm^{-1}) [39-42].

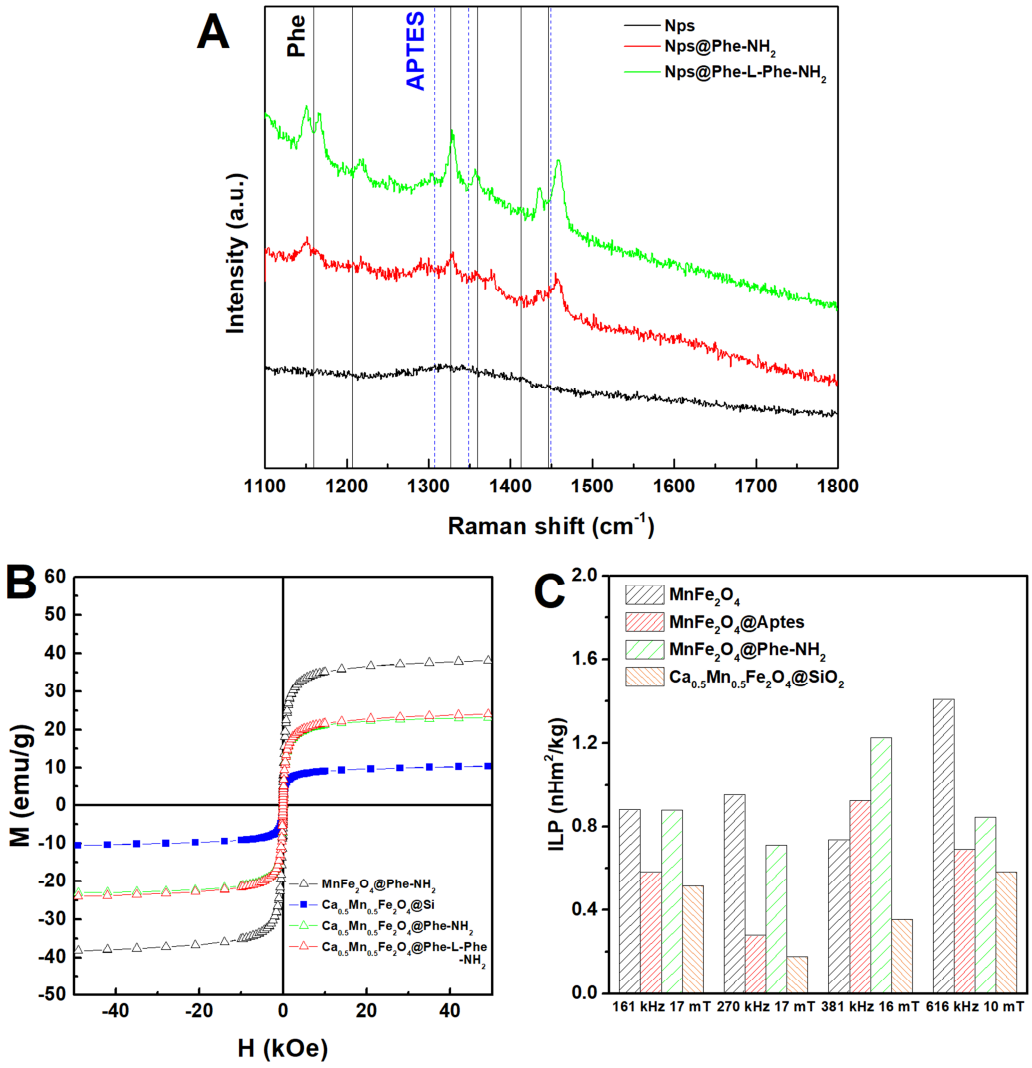

Figure S16. (A) Raman scattering spectra (1100-1800 cm^{-1} range) of the bare nanoparticles (Nps) and those functionalized with phenylalanine (Nps@Phe-NH_2) and diphenylalanine (Nps@Phe-L-Phe-NH_2). The vertical lines represent the reported Raman shifts of phenylalanine (Phe, black) and APTES (blue). (B) Magnetization hysteresis loops of functionalized nanoparticles measured at room temperature (T=300 K) and silica coated calcium-doped manganese ferrite nanoparticles. (C) Intrinsic loss power (ILP) calculated from the temperature variation over time of functionalized manganese ferrite nanoparticles and silica coated calcium-doped manganese ferrite nanoparticles in water (1 mg/mL) under different magnetic field strengths and frequencies.

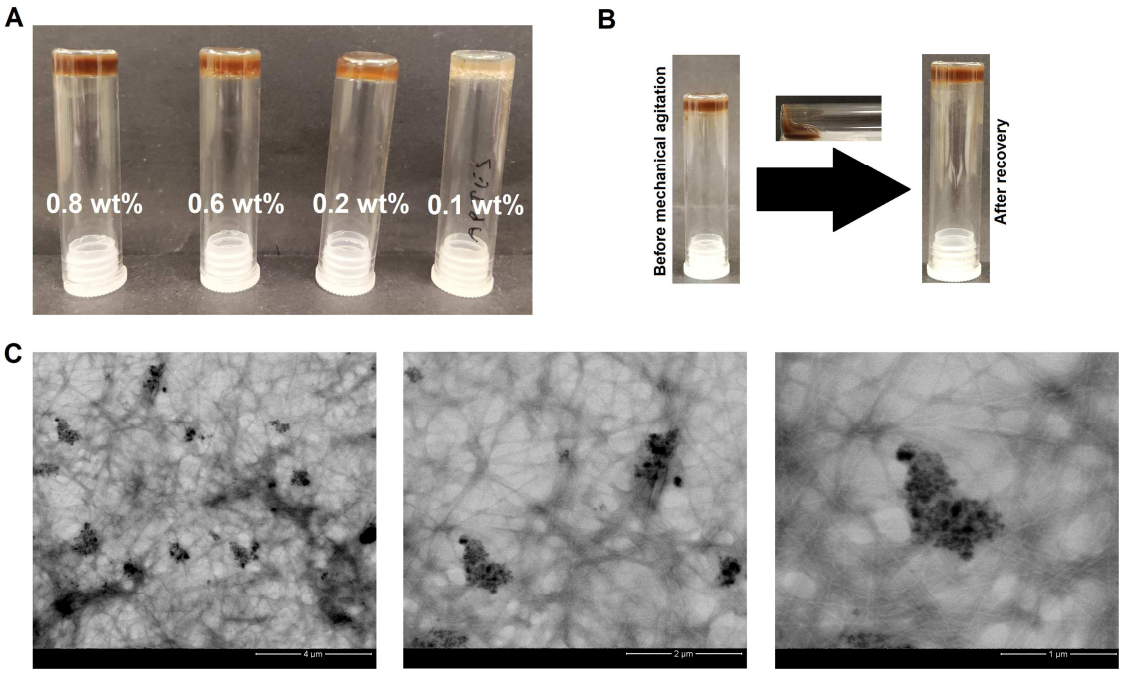

Figure S17. (A) Images of magnetic gels at different nanoparticle (calcium-doped manganese ferrite coated with APTES) content and (B) at high nanoparticle content (0.8 wt%) before and after breakage. (C) Transmission Electron Microscopy images at lower content (0.1 wt%) of nanoparticles. The gels were prepared with 0.5 wt% of hydrogelator and 0.4 wt% of GdL.

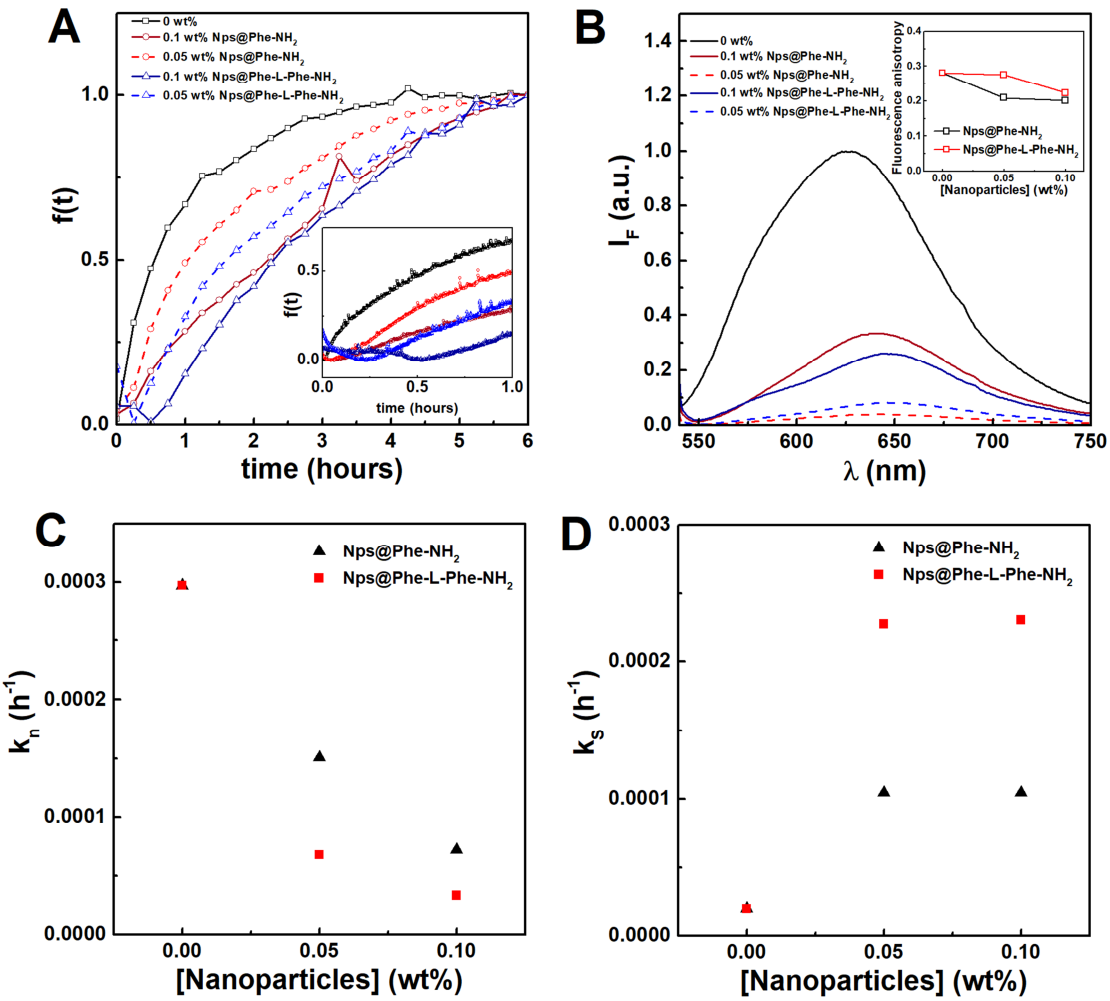

Figure S18. (A) Fluorescence emission kinetics of gel loaded with Nile Red (2 µM, λ_{exc} = 520 nm, λ_{em} = 620 nm) and various concentrations of functionalized nanoparticles. Inset: first hour of the gelation kinetics. The initial decrease of fluorescence emission in the lag phase can be associated with the assembly between nanoparticles and fibres, which is not observed in neat gels or lipogels. (B) Fluorescence emission of Nile Red (2 µM, λ_{exc} = 520 nm, λ_{em} = 620 nm) in gels with various concentrations of functionalized nanoparticles. Inset: Nile Red fluorescence anisotropy dependence on the particles' concentration. (C,D) Kinetic parameters obtained from the fitting of the Saitô's fractional aggregation model to the fluorescence kinetics data. The parameter k_s is the effective growth rate, and k_n is the nucleation rate.

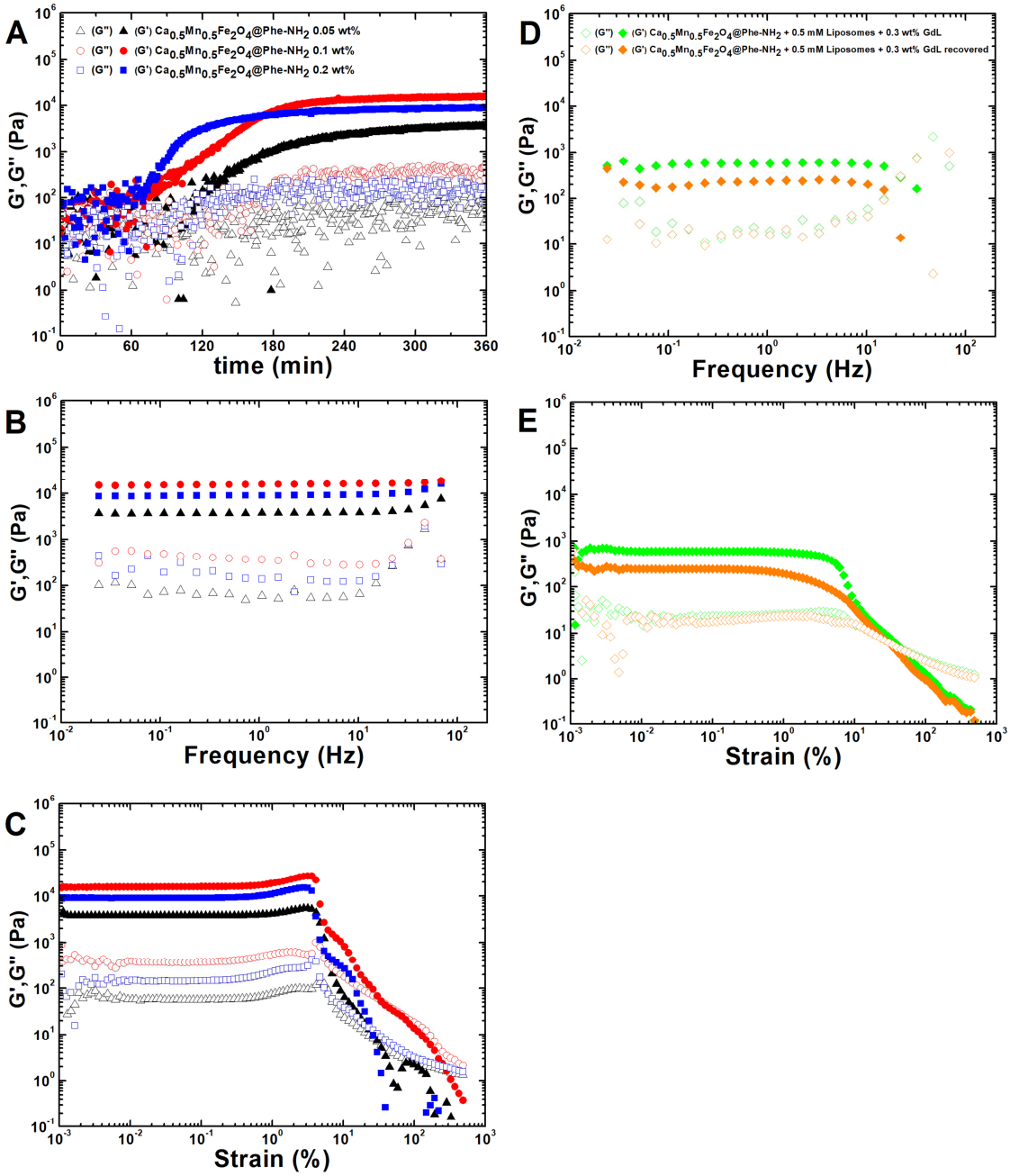

Figure S19. (A) Shear storage G' (filled symbols) and loss G'' (empty symbols) modulus during the kinetic process of gelation, (B) frequency sweep and (C) strain sweep of magnetogels (0.5 wt% hydrogelator; 0.4 wt% GdL) bearing manganese ferrite nanoparticles coated with phenylalanine ($MnFe_2O_4$@Phe-NH_2) at different concentration (0.05 wt%, 0.1 wt% and 0.2 wt%). (D,E) Shear storage G' (filled symbols) and loss G'' (empty symbols) modulus dependence during frequency and strain sweep before and 3 hours after breaking (recovered) of magnetogels (0.5 wt% hydrogelator, 0.3 wt% GdL) prepared with 0.1 wt% of calcium-doped manganese ferrites coated with phenylalanine and 0.5 mM of liposomes.

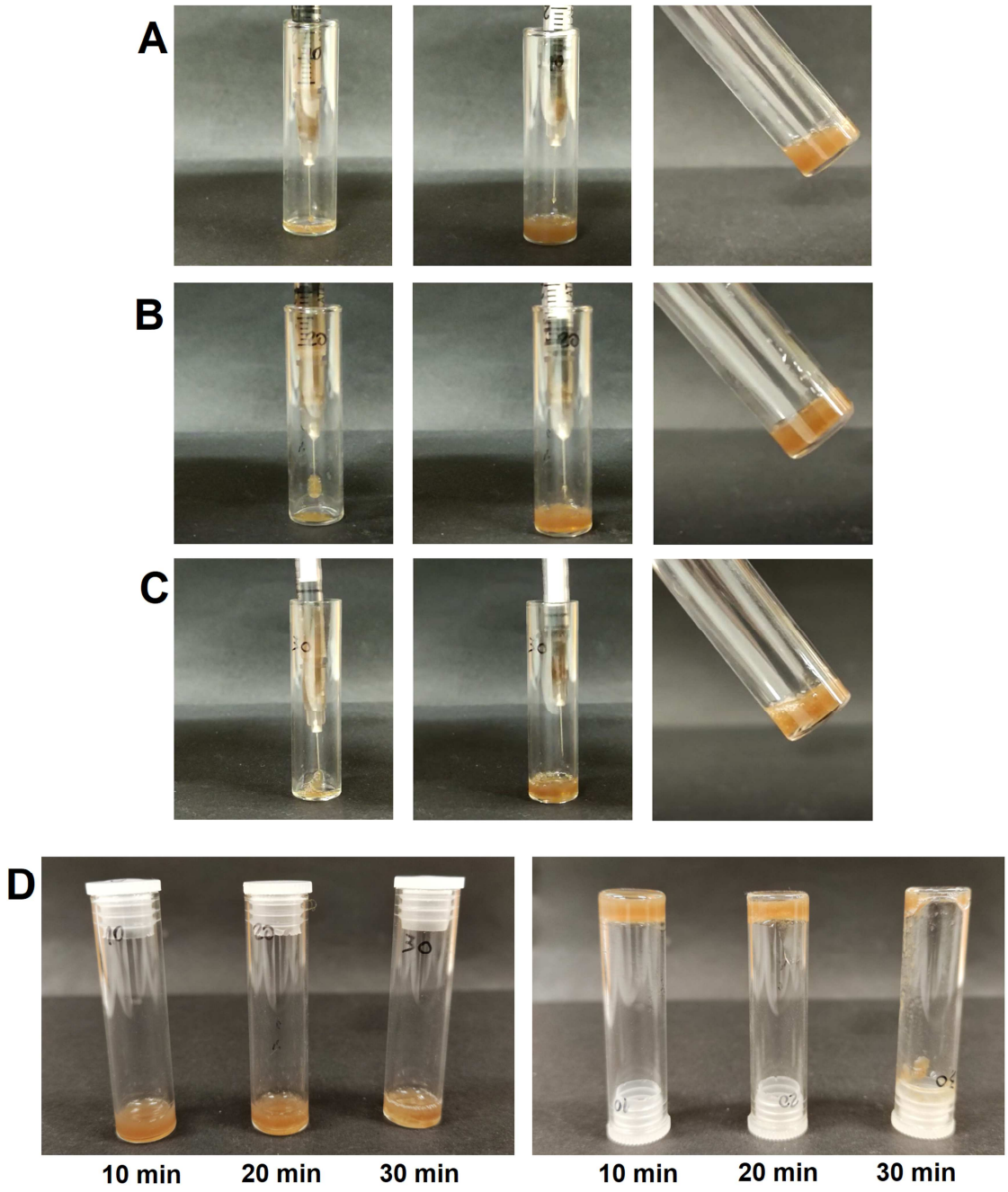

Figure S20. (A,B,C) Sequential images of the magnetogel injection at 10, 20 and 30 min after inducing gelation. (D) Vial inversion of injected magnetic gel solutions 35 min post-triggered gelation. Despite the sample B forming a gel it displayed some inhomogeneities, while the sample A was homogeneous. The sample C displayed phase separation between water and gel after injection.

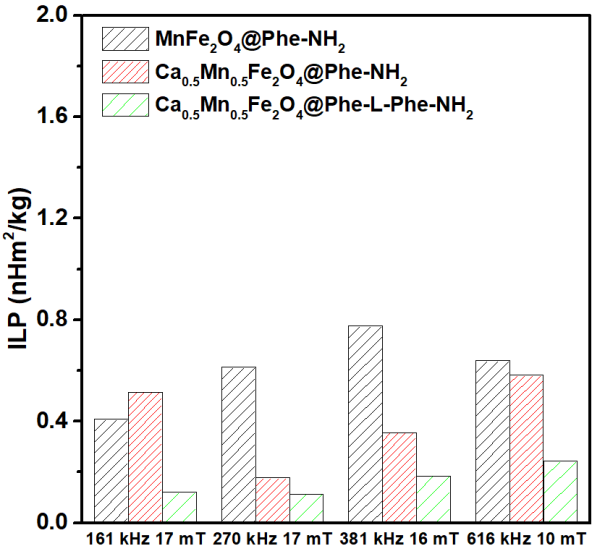

Figure S21. Intrinsic loss power (ILP) calculated from the temperature variation over time of functionalized nanoparticles (1 mg/mL) in gels (0.5 wt% hydrogelator, 0.4 wt% GdL) under different magnetic field strengths and frequencies.

Passive and active doxorubicin release

Table S4. Coefficients of determination (R^2) obtained for doxorubicin release profiles (0.1 mM) in magneto(lipo)gels with different composites. The blank spaces correspond to negative coefficients.

System	Particle	First-order	Hixson-Crowell	Higuchi	Korsmeyer-Peppas	Gompertz
Hydrogel	-	0.67	0.52	0.92	0.97	0.99
Lipogel	-	0.85	0.49	0.94	0.96	0.99
Magnetogel	0.1 wt% $Ca_{0.5}Mn_{0.5}Fe_2O_4$@Phe-NH_2	0.77	-	0.88	0.95	0.99
	0.3 wt% $Ca_{0.5}Mn_{0.5}Fe_2O_4$@Phe-NH_2	0.78	-	0.88	0.96	0.99
	0.1 wt% $Ca_{0.5}Mn_{0.5}Fe_2O_4$@Phe-L-Phe-NH_2	0.81	-	0.92	0.97	0.99
	0.3 wt% $Ca_{0.5}Mn_{0.5}Fe_2O_4$@Phe-L-Phe-NH_2	0.74	-	0.80	0.96	0.99
	0.1 wt% $MnFe_2O_4$@Phe-NH_2	0.66	-	0.61	0.93	0.98
Magneto-lipogel	0.1 wt% $Ca_{0.5}Mn_{0.5}Fe_2O_4$@Phe-NH_2	0.81	-	0.88	0.95	0.97
	0.1 wt% $Ca_{0.5}Mn_{0.5}Fe_2O_4$@Phe-L-Phe-NH_2	0.66	-	0.55	0.94	0.99
	0.1 wt% $MnFe_2O_4$@Phe-NH_2	0.66	-	0.68	0.92	0.98

The Gompertz and Korsmeyer-Peppas models are described according to the equations:

$$X_t = X_{max} e^{-ae^{b \log_{10} t}} \quad \text{(S4)}$$

$$C_t = C_0 K_s t^n \quad \text{(S5)}$$

where X_t and X_{max} are the dissolved fractions at time *t* and its maximum, a is a shape parameter and b is the dissolution rate per unit of time [55]. The C_0 and C_t are the concentrations at time 0 and *t*, and K_s is the rate constant. When $n < 0.45$, the release mechanism is diffusion-controlled (Fickian release), $0.45 < n < 0.89$ indicates a combination of diffusion and erosion drug release (non-Fickian release), $0.89 < n < 1$ indicates a relaxation-controlled release, and if $n > 1$, the release is controlled by swelling and polymer chain relaxation [55,56].

Table S5. Release coefficients of the Korsmeyer-Peppas and Gompertz models obtained for doxorubicin release profiles (0.1 mM) in magneto(lipo)gels with different composites.

		Korsmeyer-Peppas			Gompertz			
System	**Particle**	K_S	n	R^2	X_{max}	**a**	**b**	R^2
Hydrogel	-	0.00648	0.41	0.97	0.05	2.46	0.82	0.99
Lipogel	-	0.00687	0.48	0.96	0.06	2.89	1.14	0.99
Magnetogel	0.2 wt% $Ca_{0.5}Mn_{0.5}Fe_2O_4$@Phe-NH_2	0.00604	0.39	0.95	0.03	2.19	1.26	0.99
	0.3 wt% $Ca_{0.5}Mn_{0.5}Fe_2O_4$@Phe-NH_2	0.00282	0.38	0.96	0.02	2.21	0.94	0.99
	0.2 wt% $Ca_{0.5}Mn_{0.5}Fe_2O_4$@Phe-L-Phe-NH_2	0.00413	0.41	0.97	0.03	2.40	0.90	0.99
	0.3 wt% $Ca_{0.5}Mn_{0.5}Fe_2O_4$@Phe-L-Phe-NH_2	0.00432	0.34	0.96	0.02	1.86	0.99	0.99
	0.1 wt% $MnFe_2O_4$@Phe-NH_2	0.00181	0.29	0.93	0.01	1.68	0.81	0.98
Magneto-lipogel	0.2 wt% $Ca_{0.5}Mn_{0.5}Fe_2O_4$@Phe-NH_2	0.00509	0.39	0.95	0.04	2.40	0.73	0.97
	0.2 wt% $Ca_{0.5}Mn_{0.5}Fe_2O_4$@Phe-L-Phe-NH_2	0.01021	0.28	0.94	0.03	1.44	1.10	0.99
	0.2 wt% $MnFe_2O_4$@Phe-NH_2	0.00245	0.31	0.92	0.01	1.66	1.40	0.98

Table S6. Release coefficients of the Korsmeyer-Peppas model obtained for doxorubicin release profiles (0.1 mM) in magneto(lipo)gels with different composites for the first 6 h of drug release.

		Korsmeyer-Peppas		
System	**Particle**	K_S	n	R^2
Hydrogel	-	0.00477	0.66	0.99
Lipogel	-	0.00416	0.86	0.99
Magnetogel	0.3 wt% $Ca_{0.5}Mn_{0.5}Fe_2O_4$@Phe-NH_2	0.00395	0.76	0.99
	0.3 wt% $Ca_{0.5}Mn_{0.5}$ Fe_2O_4@Phe-NH_2	0.00209	0.63	0.99
	0.3 wt% $Ca_{0.5}Mn_{0.5}$ Fe_2O_4@Phe-L-Phe-NH_2	0.00305	0.67	0.99
	0.3 wt% $Ca_{0.5}Mn_{0.5}$ Fe_2O_4@Phe-L-Phe-NH_2	0.00336	0.59	0.99
	0.1 wt% $MnFe_2O_4$@Phe-NH_2	0.00145	0.52	0.99
Magneto-lipogel	0.3 wt% $Ca_{0.5}Mn_{0.5}Fe_2O_4$@Phe-NH_2	0.00360	0.70	0.99
	0.3 wt% $Ca_{0.5}Mn_{0.5}Fe_2O_4$@Phe-L-Phe-NH_2	0.00806	0.52	0.99
	0.3 wt% $MnFe_2O_4$@Phe-NH_2	0.00176	0.62	0.99

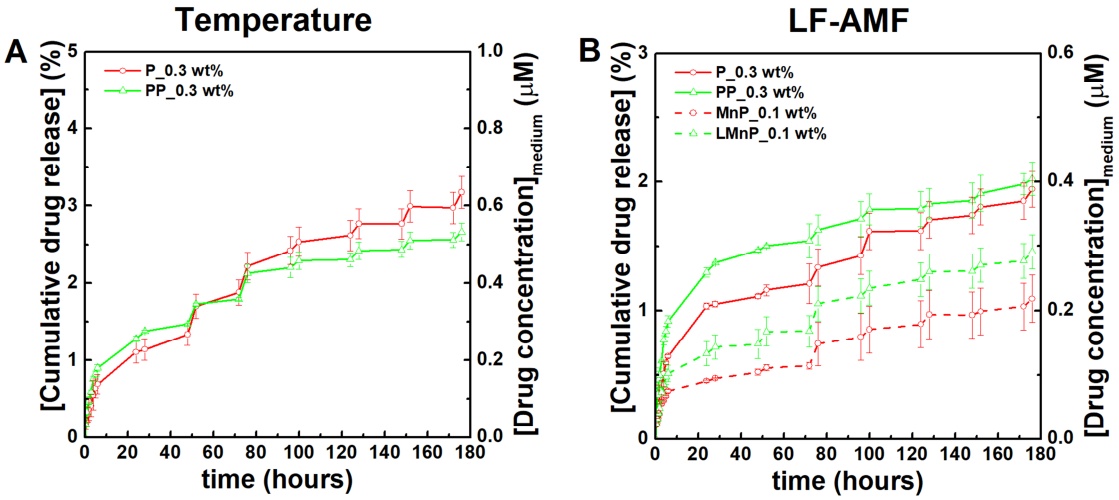

Figure S22. Cumulative doxorubicin release from magnetogels containing phenylalanine (P) and diphenylalanine (PP) functionalized calcium-doped manganese ferrite nanoparticles (0.3 wt%) to phosphate buffer pH=7.4, and from magneto(lipo)gels ((L)MnP) containing phenylalanine functionalized manganese ferrite nanoparticles (0.1 wt%). The gels were subjected either to a heating cycle (45 °C) carried out for 1 h with an interval of 24 h or a low-frequency magnetic field (LF-AMF) for 2 hours. The first cycle was initiated after 48 h of passive release. The concentration of doxorubicin in gels is 100 µM, and the maximum that can be accumulated in the medium is 20 µM (200 µL gel for 800 buffer medium).

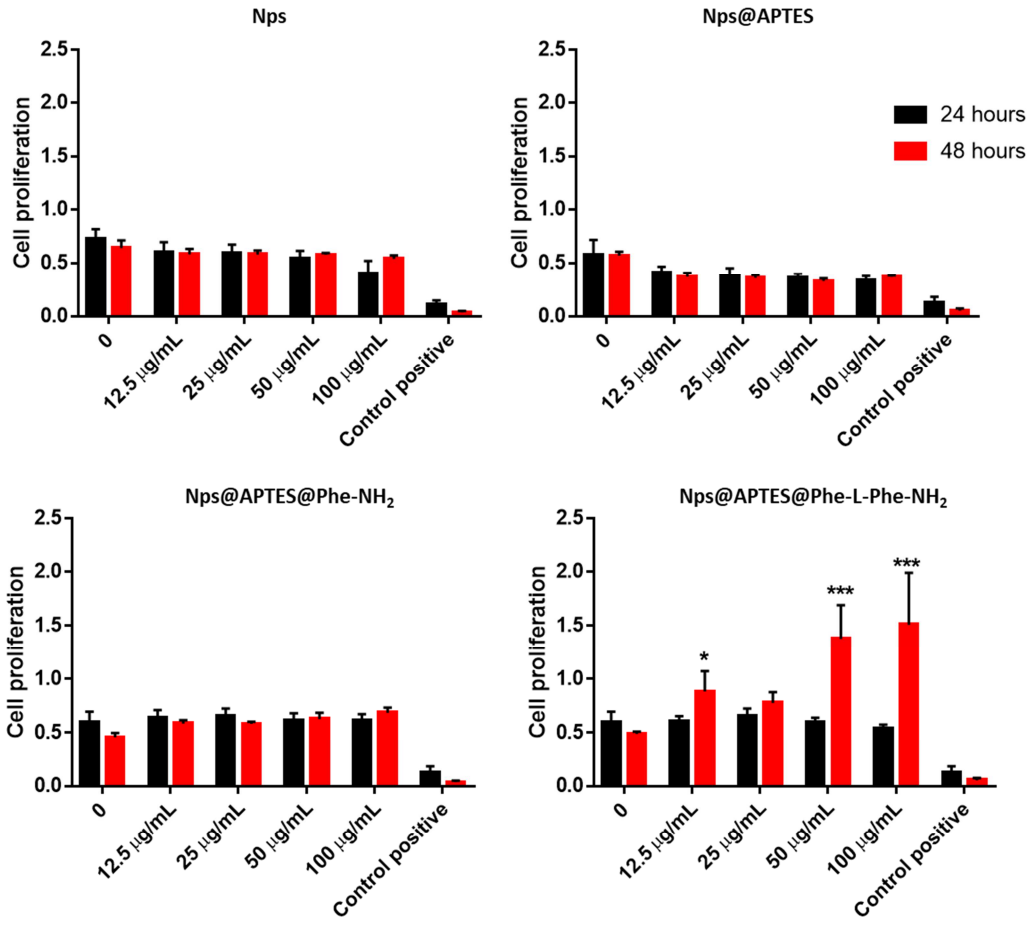

Figure S23. In vitro cell proliferation assays of magnetic nanoparticles with the core of calcium-doped manganese ferrite (Nps) functionalized with APTES, phenylalanine and diphenylalanine performed with human neuroblastoma cell line SH-SY5Y by the MTT assay. Data is represented as mean ± SD, and n = 12. *Denotes significant difference between sample and control groups ($p < 0.05$).

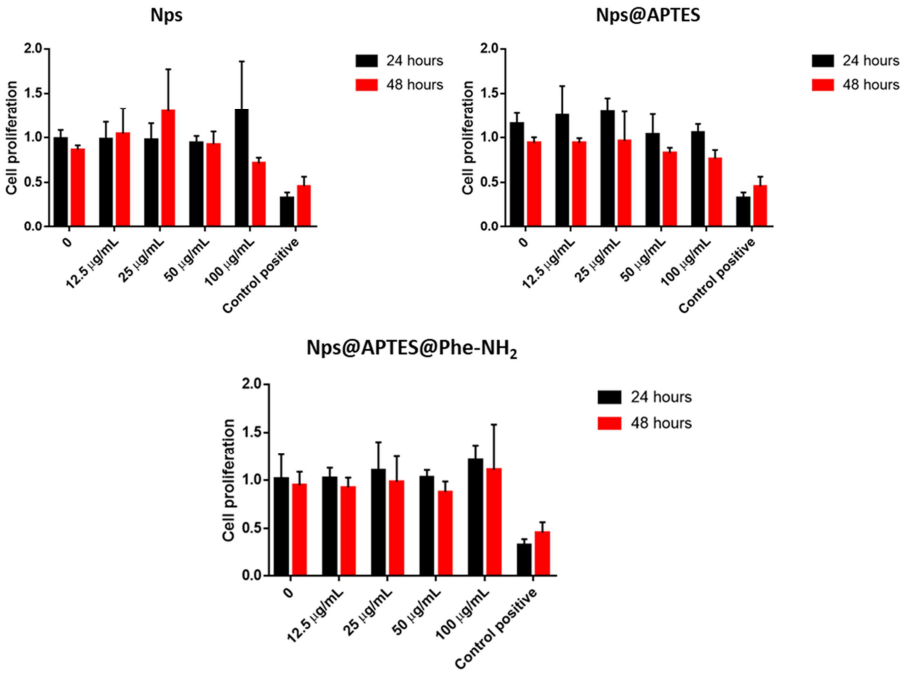

Figure S24. In vitro cell proliferation assays of magnetic nanoparticles with the core of manganese ferrite (Nps) functionalized with APTES and phenylalanine performed with U373 MG human glioblastoma cell line by the MTT assay. Data is represented as mean ± SD, and n = 12. *Denotes significant difference between sample and control groups ($p < 0.05$).

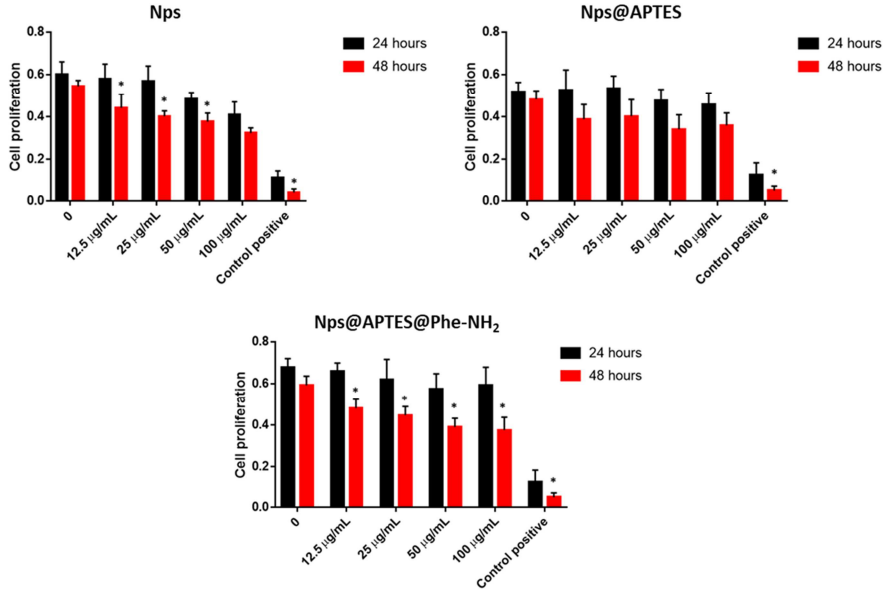

Figure S25. In vitro cell proliferation assays of magnetic nanoparticles with the core of manganese ferrite (Nps) functionalized with APTES and phenylalanine performed with human neuroblastoma cell line SH-SY5Y by the MTT assay. Data is represented as mean ± SD, and n = 12. *Denotes significant difference between sample and control groups ($p < 0.05$).

References*

1 Gaussian 09, Revision A.02, M. J. Frisch, G. W. Trucks, H. B. Schlegel, G. E. Scuseria, M. A. Robb, J. R. Cheeseman, G. Scalmani, V. Barone, B. Mennucci, G. A. Petersson, H. Nakatsuji, M. Caricato, X. Li, H. P. Hratchian, A. F. Izmaylov, J. Bloino, G. Zheng, J. L. Sonnenberg, M. Hada, M. Ehara, K. Toyota, R. Fukuda, J. Hasegawa, M. Ishida, T. Nakajima, Y. Honda, O. Kitao, H. Nakai, T. Vreven, J. A. Montgomery Jr., J. E. Peralta, F. Ogliaro, M. Bearpark, J. J. Heyd, E. Brothers, K. N. Kudin, V. N. Staroverov, R. Kobayashi, J. Normand, K. Raghavachari, A. Rendell, J. C. Burant, S. S. Iyengar, J. Tomasi, M. Cossi, N. Rega, J. M. Millam, M. Klene, J. E. Knox, J. B. Cross, V. Bakken, C. Adamo, J. Jaramillo, R. Gomperts, R. E. Stratmann, O. Yazyev, A. J. Austin, R. Cammi, C. Pomelli, J. W. Ochterski, R. L. Martin, K. Morokuma, V. G. Zakrzewski, G. A. Voth, P. Salvador, J.J. Dannenberg, S. Dapprich, A. D. Daniels, Ö. Farkas, J. B. Foresman, J. V. Ortiz, J. Cioslowski, D. J. Fox, Gaussian, Inc., Wallingford CT, 2009.

2 W. Huang, Z. X. Lin and W. F. van Gunsteren, *J. Chem. Theory Comput.*, 2011, **7**, 1237.

3 N. Schmid, A. P. Eichenberger, A. Choutko, S. Riniker, M. Winger, A. E. Mark and W. F. van Gunsteren, *Eur. Biophys. J. Biophys. Lett.*, 2011, **40**, 843.

4 H. J. C. Berendsen, J. R. Grigera and T. P. Straatsma, *J. Phys. Chem.,* 1987, **91**, 6269.

5 M.J. Abraham, D. van der Spoel, E. Lindahl, B. Hess, and the GROMACS development team, GROMACS User Manual version 5.1.4, www.gromacs.org (2016).

6 H. J. C. Berendsen, J. P. M. Postma, W. F. Vangunsteren, A. Dinola and J. R. Haak, *J. Chem. Phys*., 1984, **81**, 3684.

7 D. van der Spoel, P. J. van Maaren and H. J. C. Berendsen, *J. Chem. Phys*., 1998, **108**, 10220.

8 B. Hess, H. Bekker, H. J. C. Berendsen and J. Fraaije, *J. Comput. Chem.*, 1997, **18**, 1463.

9 B. Szała, and A. Molski, *Biophys. Chem.*, 2019, **53**, 106219.

10 C. Hui, C. Shen, T. Yang, L. Bao, J. Tian, H. Ding, C. Li and H. J. Gao, *J. Phys. Chem. C*, 2008, **112**, 11336-11339.

11 L. Khanna and N. K. Verma, *Mater. Lett.*, 2014, **128**, 376-379.

12 S. Eissler, M. Kley, D. Bächle, G. Loidl, T. Meier and D. Samson, *J. Pept. Sci.*, 2017, **23**, 757-762.

13 B. Valeur, Molecular fluorescence – Principles and Applications, Wiley-VCH, Weinheim, Germany 2001.

14 M. Torras, C. Moya, G. A. Pasquevich and A. Roig, *Microchimica Acta*, 2020, **187**, 488.